STABLE SEMI-IMPLICIT SDC METHODS FOR CONSERVATION LAWS

JÖRG STILLER

Abstract. Semi-implicit spectral deferred correction (SDC) methods provide a systematic approach to construct time integration methods of arbitrarily high order for nonlinear evolution equations including conservation laws. They converge towards A- or even L-stable collocation methods, but are often not sufficiently robust themselves. In this paper, a family of SDC methods inspired by an implicit formulation of the Lax-Wendroff method is developed. Compared to fully implicit approaches, the methods have the advantage that they only require the solution of positive definite or semi-definite linear systems. Numerical evidence suggests that the proposed semi-implicit SDC methods with Radau points are L-stable up to order 11 and require very little diffusion for orders 13 and 15. The excellent stability and accuracy of these methods is confirmed by numerical experiments with 1D conservation problems, including the convection-diffusion, Burgers, Euler and Navier-Stokes equations.

1. Introduction

The trend towards higher-order numerical methods for conservation laws in fluid mechanics and beyond increases the need for time integration methods that match the convergence and efficiency of spatial methods. A wide range of those methods have been developed in recent decades [25, 28, 29]. They include explicit, implicit and semi-implicit methods using multiple steps, stages or derivatives [9]. Convection-dominant problems are often not stiff and can be solved with explicit methods. In particular, strong stability preserving Runge-Kutta methods are a popular choice for hyperbolic problems with discontinuous solutions [24, 43]. However, explicit methods lose efficiency when the stiffness increases due to unresolved waves, diffusion or local mesh refinement. This issue is particularly pronounced with high-order spatial finite element methods, where the diffusion time scales like P^4/h^2 for elements of size h and degree P [10]. One approach to avoid the resulting time step restrictions is to use fully implicit methods such as diagonally implicit Runge-Kutta methods [42, 54, 55], Rosenbrock methods [5], Taylor methods [3] or discontinuous Galerkin methods in time [67]. Unfortunately, these methods often lead to ill conditioned algebraic systems that are expensive to solve. In time-resolved simulations, it therefore remains a challenge to compete with explicit methods.

Semi-implicit methods take advantage of the fact that the asymmetric and often nonlinear convection terms are non-stiff and thus suited for explicit treatment. The diffusion terms usually require an implicit discretization, but are (quasi-)linear and lead to (semi-)definite algebraic systems that can be solved with standard methods of linear algebra. Popular semi-implicit methods include implicit-explicit (IMEX) multistep methods and Runge-Kutta methods. IMEX multistep methods can achieve an arbitrary order of convergence by extrapolating the non-stiff terms [35, Ch.4.2]. However, the increase in order affects stability [1, 20]. Therefore, the IMEX multistep methods used in practice rarely exceed order 3, e.g. [19, 40, 44]. IMEX Runge-Kutta methods are

TU Dresden, Institute of Fluid Mechanics, 01062 Dresden, Germany

E-mail address: joerg.stiller@tu-dresden.de.

Key words and phrases. Semi-implicit methods; Spectral deferred correction; discontinuous Galerkin method.

often a better choice because they possess a larger stability domain and a lower error constant than comparable multistep methods [2, 12, 37, 41]. By using them as a partitioned scheme, IMEX Runge methods also allow for the semi-implicit treatment of quasi-linear stiff terms [6]. This approach was recently applied to compressible and incompressible Navier-Stokes problems [7, 26]. However, due to the increasingly complex order conditions, it is difficult to increase the rate of convergence and there is no known IMEX Runge-Kutta method with an order higher than 5.

Recently, considerable progress in developing higher order semi-implicit time integration methods was achieved using multi-derivative methods, e.g. [21, 50, 58]. Alternatively, spectral deferred correction (SDC) methods can be used to construct schemes of arbitrary high order [18]. Semi-implicit SDC methods were proposed by Minion [52] and further developed in [14, 15, 27, 47]. In recent applications to incompressible Navier-Stokes problems, these methods achieved temporal convergence rates up to 12 [51, 66]. For laminar flow problems, semi-implicit SDC methods proved competitive with IMEX multistep and Runge-Kutta methods for relative L^2 errors below 10^{-4} . However, in direct simulations of turbulent flows, where non-linear convective processes dominate, the SDC methods suffered from instabilities [26].

For improving the usability of semi-implicit SDC methods it is imperative to increase their stability. To achieve this goal, a novel approach is proposed in this paper. It divides the convection term into a possibly nonlinear explicit part and an implicitly treated diffusion-like part. This splitting is inspired by the Lax-Wendroff method, where the two parts appear as the first terms of a Taylor (or Cauchy-Kovalevskaya) expansion [46]. The main difference consists in the implicit treatment of the diffusion-like part. A similar strategy was already used in Taylor-Galerkin methods [17, 57], streamline-upwind Petrov-Galerkin methods [8, 34] and multi-derivative methods [21, 39]. In contrast to these methods, however, the present work does not extend the Taylor series expansion to the physical diffusion terms. Instead, the incomplete expansion is used to design *L*-stable time integrators, from which robust high-order SDC methods are constructed. Due to the different treatment of the convection term, these SDC methods are three-quarter-implicit rather than semi-implicit. Nevertheless, they require only the solution of well-posed linear algebraic equations and thus share the advantages of conventional semi-implicit methods.

An outline of the paper follows: Section 2 gives a brief overview of the one-dimensional conservation laws considered. The first part of Section 3 is concerned with the development of robust semi-implicit one- and two-stage integrators. In the second part, SDC methods based on these integrators are constructed and analyzed. Spatial discretization including stabilization techniques is described in Section 4, followed by a brief discussion of solution methods in Section 5. Section 6 provides numerical experiments for convection-diffusion, Burgers, and compressible flow problems. Conclusions are drawn in Section 7.

2. Conservation laws

2.1. Conservation systems in one space dimension. Consider the one-dimensional conservation law

$$\partial_t \mathbf{u} = -\partial_x \mathbf{f}_{c}(\mathbf{u}) + \partial_x \mathbf{f}_{d}(\mathbf{u}) + \mathbf{f}_{s}(\mathbf{u}, x, t) =: \mathbf{f}(\mathbf{u}, x, t)$$
(1)

for $x \in \Omega \subset \mathbb{R}$ and $t \in \mathbb{R}^+$, where $\textbf{\textit{u}}(x,t) \in \mathbb{R}^d$ are the conservative variables, $\textbf{\textit{f}}_c$ the convective fluxes, $\textbf{\textit{f}}_d$ the diffusive fluxes, $\textbf{\textit{f}}_s$ the sources and $\textbf{\textit{f}}$ is the combined right-hand side. It is assumed that the convective fluxes possess the Jacobian $\textbf{\textit{A}}_c = \textbf{\textit{f}}_c'(\textbf{\textit{u}})$ and the diffusive fluxes can be written in the form $\textbf{\textit{f}}_d = \textbf{\textit{A}}_d \partial_x \textbf{\textit{u}}$, where $\textbf{\textit{A}}_d(\textbf{\textit{u}}, \partial_x \textbf{\textit{u}})$ is the positive-semidefinite diffusion matrix. These definitions yield the quasilinear form

$$\partial_t \mathbf{u} = -\mathbf{A}_c \partial_x \mathbf{u} + \partial_x \mathbf{A}_d \partial_x \mathbf{u} + \mathbf{f}_s$$
.

2.2. Scalar conservation laws. Scalar laws consist of only one conservation equation with solution u such that u = [u]. Two cases are considered. The first is the convection-diffusion equation

$$\partial_t u = -\partial_x (vu) + \partial_x (v\partial_x u) \tag{2}$$

with constant velocity v and diffusivity $v \ge 0$. This yields the convective Jacobian $\mathbf{A}_{\rm c} = [v]$ and the diffusion matrix $\mathbf{A}_{\rm d} = [v]$. The second case is the Burgers equation

$$\partial_t u = -\partial_x \left(\frac{1}{2}u^2\right) + \partial_x (v\partial_x u) + f_s(x,t)$$

with constant diffusivity $v \ge 0$, convective Jacobian $\mathbf{A}_c = [u]$ and diffusion matrix $\mathbf{A}_d = [v]$. The source f_s can be manufactured to match a prescribed exact solution.

2.3. Euler and Navier-Stokes equations. For the Navier-Stokes equations, the conservative variables, convective fluxes and diffusive fluxes given by

$$\boldsymbol{u} = \begin{bmatrix} \rho \\ \rho v \\ \rho E \end{bmatrix}, \quad \boldsymbol{f}_{c} = \begin{bmatrix} \rho v \\ \rho v^{2} + p \\ \rho v E + p v \end{bmatrix}, \quad \boldsymbol{f}_{d} = \begin{bmatrix} 0 \\ \frac{4}{3} \eta \partial_{x} v \\ \frac{4}{3} \eta v \partial_{x} v + \lambda \partial_{x} T \end{bmatrix},$$

where ρ is the density, v the velocity, E the total specific energy, η the dynamic viscosity and λ the heat conductivity. Assuming a perfect gas with the gas constant $R = c_p - c_v$ and the ratio of the specific heats $\gamma = c_p/c_v$ it is possible to calculate the temperature $T = (E - v^2/2)/c_v$, the pressure $p = \rho RT$, the total specific enthalpy $H = E + p/\rho$ and the speed of sound $a = ((\gamma - 1)RT)^{1/2}$. The convective Jacobian and the diffusion matrix are given by

$$\mathbf{A}_{c} = \begin{bmatrix} 0 & 1 & 0 \\ \frac{1}{2}(\gamma - 3)v^{2} & (3 - \gamma)v & \gamma - 1 \\ \frac{1}{2}(\gamma - 1)v^{3} - vH & H - (\gamma - 1)v^{2} & \gamma v \end{bmatrix}$$

and

$$\boldsymbol{A}_{\mathrm{d}} = \begin{bmatrix} 0 & 0 & 0 \\ -\frac{4}{3}vv & \frac{4}{3}v & 0 \\ -\left(\frac{4}{3}v - \gamma\kappa\right)v^2 - \gamma\kappa E & \left(\frac{4}{3}v - \gamma\kappa\right)v & \gamma\kappa \end{bmatrix},$$

where $v = \eta/\rho$ is the kinematic viscosity and $\kappa = \lambda/(\rho c_p)$ the thermal diffusivity. The inviscid case with $\eta = \lambda = 0$ leads to the Euler equations for which $\mathbf{A}_{\rm d} = \mathbf{0}$.

3. Time integration

3.1. Semi-explicit integrators of order 1 and 2. This section provides low-order time integrators as building blocks for SDC methods. The aim is to devise a semi-implicit approach that avoids the fully implicit treatment of convection, but achieves A-stability and exhibits a robust behavior when applied to nonlinear conservation laws. For readability, the dependence on x is hidden throughout the section, except for the spatial derivatives.

As the starting point consider the purely convective system

$$\partial_t \mathbf{u} + \partial_x \mathbf{f}_{\mathbf{c}}(\mathbf{u}) = 0. \tag{3}$$

The application of the Lax-Wendroff method [46] to (3) yields

$$\frac{\mathbf{u}^{n+1} - \mathbf{u}^n}{\Delta t} + \partial_x \mathbf{f}_{c}(\mathbf{u}^n) = \partial_x \frac{\Delta t}{2} \mathbf{A}_{c}^{2}(\mathbf{u}^n) \, \partial_x \mathbf{u}^n \,,$$

where $\Delta t = t^{n+1} - t^n$ is the time step size and $u^n \approx u(t^n)$. This scheme is second-order accurate but only conditionally stable. To improve the stability, the right-hand side can be changed to a semi-implicit form such that

$$\frac{\boldsymbol{u}^{n+1} - \boldsymbol{u}^n}{\Delta t} + \partial_x \boldsymbol{f}_{c}(\boldsymbol{u}^n) = \partial_x \frac{\Delta t}{2} \boldsymbol{A}_{c}^{2}(\boldsymbol{u}^n) \, \partial_x \boldsymbol{u}^{n+1} \,. \tag{4}$$

The modified scheme retains order 2 and proves unconditionally stable for linear convection with constant velocity (see Sec. 3.1.3). Its implicit part corresponds to a diffusion problem, which yields a positive-definite linear system when discretized in space. Therefore, the discrete equations are significantly easier to solve than the nonlinear or indefinite systems that emerge from fully implicit methods.

Unfortunately, there exists no straightforward extension of the Lax-Wendroff method to conservation laws including diffusion. Constructing a corresponding single stage method of order 2 would imply the introduction of third derivatives as in Taylor-Galerkin methods or multiderivative methods, see e.g. [17, 29]. The methods proposed below avoid this complication by introducing further stages.

3.1.1. Integrators of order 1. For concise notation, the functionals

$$\phi_{\rm ex}(\mathbf{u}^{\alpha}) = -\partial_{x} f_{\rm c}(\mathbf{u}^{\alpha}), \tag{5a}$$

$$\boldsymbol{\phi}_{\text{im}}(\boldsymbol{u}^{\alpha}, \boldsymbol{u}^{\beta}, t, \theta) = \partial_{x} \left(\left(\frac{\theta}{2} \boldsymbol{A}_{c}^{2} (\boldsymbol{u}^{\alpha}) + \boldsymbol{A}_{d} (\boldsymbol{u}^{\alpha}) \right) \partial_{x} \boldsymbol{u}^{\beta} \right) + \boldsymbol{f}_{s} (\boldsymbol{u}^{\alpha}, x, t)$$
 (5b)

are introduced to distinguish the explicit and implicit contributions of convection, diffusion and sources to the semi-discrete equations. In (5) the arguments $\boldsymbol{u}^{\alpha}(x)$ and $\boldsymbol{u}^{\beta}(x)$ represent different instances of the semi-discrete solution or approximations to it, while θ is a parameter which corresponds to an interval in time. The explicit dependence of $\boldsymbol{\phi}_{\text{im}}$ on x is dropped for brevity.

Using these definitions and accounting for ${\pmb A}_{\rm d}={\pmb 0}$, the modified Lax-Wendroff method (4) can be rewritten in the form

$$\mathbf{u}^{n+1} = \mathbf{u}^n + \Delta t \left[\phi_{\text{ex}}(\mathbf{u}^n) + \phi_{\text{im}}(\mathbf{u}^n, \mathbf{u}^{n+1}, t^{n+1}, \Delta t) \right].$$
 (6)

Given the above definition for $\phi_{\rm im}$, this scheme applies also to convective-diffusive conservation laws (1), for which it yields a backward Euler discretization of the diffusion term. Sources are treated implicitly if they are independent of the solution and explicitly otherwise. In summary, (6) can be characterized one-stage semi-implicit time integrator of order 1. For simplicity, the method is referred to as SI1(1) in the following.

Although SI1(1) has excellent stability properties (see Sec. 3.1.3), a stronger damping was found to be necessary in high-order SDC methods. This is achieved by a second stage in which the result of (6) is used to update the explicit part of the RHS. The resulting two-stage first-order method SI1(2) is given by

$$u^{(1)} = u^{n} + \Delta t \left[\phi_{ex}(u^{n}) + \phi_{im}(u^{n}, u^{(1)}, t^{n+1}, \Delta t) \right],$$

$$u^{(2)} = u^{n} + \Delta t \left[\phi_{ex}(u^{(1)}) + \phi_{im}(u^{n}, u^{(2)}, t^{n+1}, \Delta t) \right],$$

$$u^{n+1} = u^{(2)}.$$
(7)

Using Taylor expansion, it can be shown that the second stage adds a term of the form $\partial_x(\Delta t \boldsymbol{A}_c^2 \partial_x \boldsymbol{u})$, which is about twice the amount of numerical diffusion introduced by the Euler backward method. A similar effect could be achieved without a second stage by including an artificial diffusion term in SI1(1). However, comparative studies have shown that this approach is less efficient.

3.1.2. *Integrator of order 2.* To obtain a method of order 2, SI1(2) can be modified by performing two half steps followed by the application of the midpoint rule. This yields the semi-implicit two-stage method SI2(2)

$$\mathbf{u}^{(1)} = \mathbf{u}^{n} + \frac{\Delta t}{2} \left[\phi_{\text{ex}}(\mathbf{u}^{n}) + \phi_{\text{im}}(\mathbf{u}^{n}, \mathbf{u}^{(1)}, t^{n} + \Delta t/2, \Delta t) \right],$$

$$\mathbf{u}^{(2)} = \mathbf{u}^{n} + \frac{\Delta t}{2} \left[\phi_{\text{ex}}(\mathbf{u}^{(1)}) + \phi_{\text{im}}(\mathbf{u}^{n}, \mathbf{u}^{(2)}, t^{n} + \Delta t/2, \Delta t) \right],$$

$$\mathbf{u}^{n+1} = \mathbf{u}^{n} + \Delta t f(\mathbf{u}^{(2)}, t^{n} + \Delta t/2).$$

Another two-stage second-order method can be constructed using the trapezoidal rule. However, this method is less stable and therefore not pursued any further.

3.1.3. Linear stability of semi-implicit integrators. Consider the convection-diffusion equation (2) with the spatially periodic complex solution $u = \hat{u}(t)e^{ikx}$. Evaluating the spatial derivatives and removing the common factor e^{ikx} yields

$$d_t \hat{u} = -ivk\hat{u} - vk^2\hat{u}. \tag{8}$$

This equation is equivalent to the Dahlquist equation

$$d_{,}\hat{u} = \lambda \hat{u}, \tag{9}$$

where $\lambda \in \mathbb{C}$ with the real part $\lambda_{\rm r} = -vk^2$ and imaginary part $\lambda_{\rm i} = -vk$. The application of a one-step method to (9) yields the stability function

$$R(z) = \frac{\hat{u}^{n+1}}{\hat{u}^n} \,,$$

where $z = \Delta t \lambda$. The set $\{z \in \mathbb{C}; |R(z)| \le 1\}$ is the stability domain of the method. The method is called *A*-stable if $|R(z)| \le 1$ for all *z* with $z_i \le 0$ and *L*-stable if in addition R = 0 for $z \to \infty$.

Remark 1. For conservation laws, $|z_i| = \Delta t |v| k$ can be associated with the CFL number and $-z_r = \Delta t v k^2$ with the diffusion number of the fully discrete problem.

To apply the one-step methods presented above to the model problem (8), it is necessary to identify the amplitudes of the explicit and implicit RHS parts defined in (5). Substituting the solution, evaluating the derivative and separating the factor e^{ikx} gives

$$\begin{split} \hat{\phi}_{\text{ex}}(\hat{u}) &= i\lambda_i \, \hat{u} \,, \\ \hat{\phi}_{\text{im}}(\hat{u}, \theta) &= \left(\lambda_r - \frac{\theta}{2}\lambda_i^2\right) \hat{u} \,. \end{split}$$

With these ingredients, the one-stage first-order method SI1(1) yields

$$\hat{u}^{n+1} = \hat{u}^n + \Delta t \left[\hat{\phi}_{\text{ex}}(\hat{u}^n) + \hat{\phi}_{\text{im}}(\hat{u}^{n+1}, \Delta t) \right]$$

or, equivalently,

$$\hat{u}^{n+1} = \hat{u}^n + iz_i\hat{u}^n + \left(z_r - \frac{1}{2}z_i^2\right)\hat{u}^{n+1}$$
.

This gives the stability function

$$R_{\text{SI1(1)}}(z) = \frac{1 + iz_i}{1 - z_r + \frac{1}{2}z_i^2}.$$
 (10)

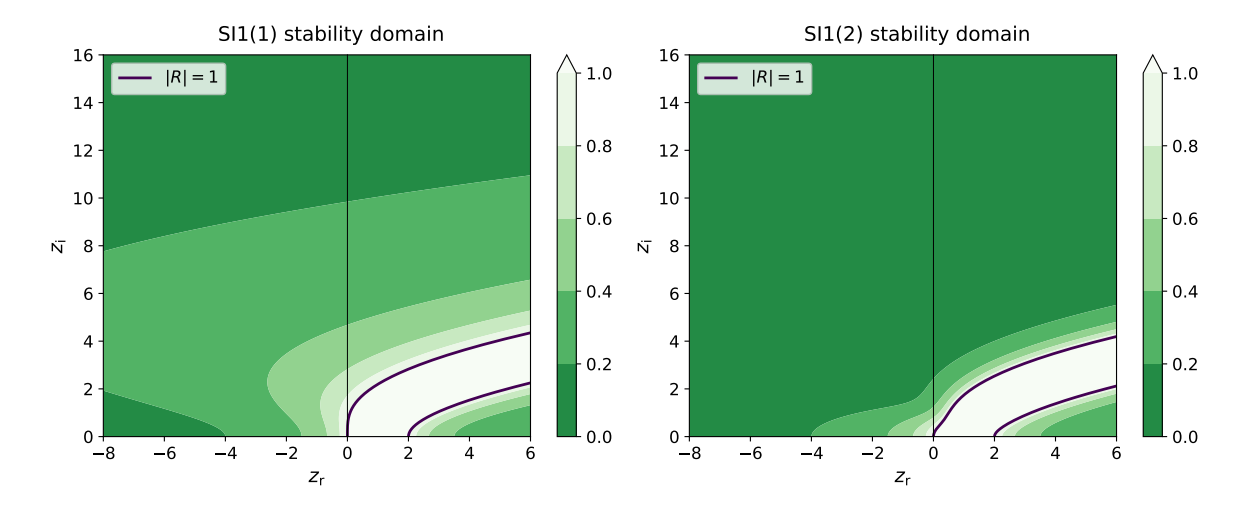


Figure 1. Stability domains of the first-order integrators

For the two-stage method SI1(2), similar considerations lead to

$$R_{\text{SI1(2)}}(z) = \frac{1 + iz_i R_{\text{SI1(1)}}(z)}{1 - z_r + \frac{1}{2} z_i^2}.$$
 (11)

The stability domains of both methods are depicted in Fig. 1. A closer inspection of the stability functions (10) and (11) yields the following result:

Proposition 1. The time integration methods SI1(1) and SI1(2) are *L*-stable.

Finally, the stability function of the second-order method SI2(2) is given by

$$R_{\text{Sl2(2)}}(z) = 1 + z \frac{1 + \frac{i}{2} z_i R_{\text{Sl2(1)}}(z)}{1 - \frac{1}{2} z_r + \frac{1}{4} z_i^2},$$

where

$$R_{\text{SI2(1)}}(z) = \frac{1 + \frac{i}{2}z_i}{1 - \frac{1}{2}z_r + \frac{1}{4}z_i^2}$$

is the stability function of the first stage. The graph of the stability domain depicted in Figure 2 indicates the following property, which can be proved by analyzing the stability function:

Proposition 2. The time integration method SI2(1) is A-stable.

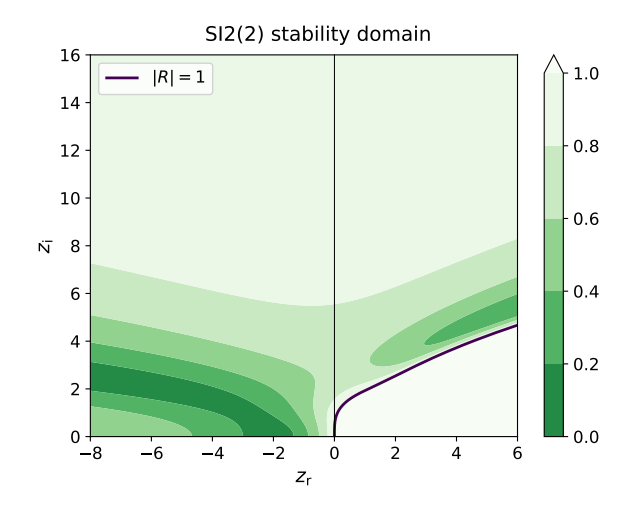


Figure 2. Stability domain of the second-order integrator

3.2. Spectral deferred correction method.

3.2.1. *SDC with right-sided Gauss-Radau points.* The SDC method seeks an approximate solution to the Picard integral equation

$$\boldsymbol{u}(t) = \boldsymbol{u}(t^n) + \int_{t^n}^t \boldsymbol{f}(\boldsymbol{u}(\tilde{t}), \tilde{t}) \, \mathrm{d}\tilde{t} \,, \quad t \in [t^n, t^{n+1}] \,. \tag{12}$$

Its key idea is to 1) replace the exact solution and the integrand by Lagrange interpolants through a set of collocation points and 2) solve the error equation by sweeping through the collocation points with a low-order method [18]. Common choices for the collocation points include Gausstype quadrature points and equidistant points [48, 53]. The following description is restricted to the right-sided Gauss-Radau points, but can easily be extended to other point sets.

Let $\underline{\tau} = {\{\tau_m\}}_{m=1}^M$ be the right Radau points in the unit interval [0,1] and

$$\ell_m(\tau) = \prod_{\substack{n=1\\n\neq m}}^M \frac{\tau - \tau_n}{\tau_m - \tau_n} \tag{13}$$

the corresponding Lagrange basis polynomials. The collocation points $\underline{t} = \{t_m\}_{m=1}^M$ in the interval $[t^n, t^{n+1}]$ result from the mapping $t_m = t(\tau_m)$, where $t(\tau) = t^n + \tau \Delta t$. The values of some quantity \boldsymbol{v} in the collocation points form the vector $\underline{\boldsymbol{v}} = [\boldsymbol{v}_n]$, which is used to construct the Lagrange interpolant

$$\boldsymbol{L}(\underline{\boldsymbol{v}},t) = \sum_{m=1}^{M} \boldsymbol{v}_{m} \, \mathcal{E}_{m}(\tau(t))$$

with $\tau(t)=(t-t^n)/\Delta t$. For a simple notation, the initial time is denoted by $t_0=t^n$ and the initial value of the solution by $\boldsymbol{u}_0=\boldsymbol{u}(t^n)$. Note, however, that t_0 is no collocation point, \boldsymbol{u}_0 is not a component of $\underline{\boldsymbol{u}}$ and generally $\boldsymbol{u}_0\neq \boldsymbol{L}(\underline{\boldsymbol{u}},t_0)$.

The SDC method starts from an initial approximation $\underline{\boldsymbol{u}}_{m}^{0} = [\boldsymbol{u}_{m}^{0}]$ that results from sweeping through all subintervals $\{[t_{m-1},t_{m}]\}_{m=1}^{M}$ with a suitable time integrator. This prediction step is followed by several correction sweeps designed to reduce the error

$$\delta(t) = \mathbf{u}(t) - \mathbf{L}(\mathbf{u}^k, t),$$

where \underline{u}^k denotes the k-th approximation. Using the Picard formulation (12) and the residual function

$$\boldsymbol{\varepsilon}(t) = \boldsymbol{u}_0 + \int_{t_0}^t \boldsymbol{f} \left(\boldsymbol{L}(\underline{\boldsymbol{u}}^k, \tilde{t}), \, \tilde{t} \right) \mathrm{d}\tilde{t} - \boldsymbol{L}(\underline{\boldsymbol{u}}^k, t)$$
(14)

the error equation

$$\boldsymbol{\delta}(t) = \boldsymbol{\varepsilon}(t) + \int_{t_0}^t \left[\boldsymbol{f} \left(\boldsymbol{L}(\underline{\boldsymbol{u}}^k, \tilde{t}) + \boldsymbol{\delta}(\tilde{t}), \, \tilde{t} \right) - \boldsymbol{f} \left(\boldsymbol{L}(\underline{\boldsymbol{u}}^k, \tilde{t}), \tilde{t} \right) \right] \mathrm{d}\tilde{t}$$

can be derived, see e.g. [52]. The difference of $\delta(t)$ at the subinterval end points results in the identity

$$\delta(t_m) = \delta(t_{m-1}) + \varepsilon(t_m) - \varepsilon(t_{m-1}) + \int_{t_{m-1}}^{t_m} \left[f\left(L(\underline{\boldsymbol{u}}^k, \tilde{t}) + \delta(\tilde{t}), \, \tilde{t}\right) - f\left(L(\underline{\boldsymbol{u}}^k, \tilde{t}), \, \tilde{t}\right) \right] d\tilde{t}. \tag{15}$$

Letting δ_m denote the approximation to $\delta(t_m)$, the discretization of (15) with the one-stage first-order integrator SI1(1) is

$$\delta_{m} = \delta_{m-1} + \varepsilon(t_{m}) - \varepsilon(t_{m-1}) + \Delta t_{m} \left[\phi_{\text{ex}} (\boldsymbol{u}_{m-1}^{k+1}) + \phi_{\text{im}} (\boldsymbol{u}_{m-1}^{k+1}, \boldsymbol{u}_{m}^{k+1}, t_{m}, \Delta t_{m}) \right] - \Delta t_{m} \left[\phi_{\text{ex}} (\boldsymbol{u}_{m-1}^{k}) + \phi_{\text{im}} (\boldsymbol{u}_{m-1}^{k}, \boldsymbol{u}_{m}^{k}, t_{m}, \Delta t_{m}) \right] ,$$
(16)

where $\Delta t_m = t_m - t_{m-1}$. With (14), the residual difference can be written

$$\varepsilon(t_m) - \varepsilon(t_{m-1}) = \int_{t_{m-1}}^{t_m} f\left(L(\underline{\boldsymbol{u}}^k, \tilde{t}), \tilde{t}\right) d\tilde{t} - \boldsymbol{u}_m^k + \boldsymbol{u}_{m-1}^k.$$
(17)

The integral in (17) is approximated using the quadrature

$$\int_{t_{m-1}}^{t_m} f\left(L(\underline{\boldsymbol{u}}^k, t), t\right) dt \approx \int_{t_{m-1}}^{t_m} L\left(\underline{\boldsymbol{f}}^k, t\right) dt = \Delta t \sum_{i=1}^{M} w_{i,m} f(\boldsymbol{u}_i^k, t_i) = S_m^k$$

with the weights

$$w_{i,m} = \int_0^{\tau_m} \ell_i(\tau) \mathrm{d}\tau.$$

Substituting (17) into (16) and defining the new approximation $\boldsymbol{u}_m^{k+1} = \boldsymbol{u}_m^k + \boldsymbol{\delta}_m$ gives the SI1(1) corrector

$$u_{m}^{k+1} = u_{m-1}^{k+1} + S_{m}^{k} + \Delta t_{m} \left[\phi_{\text{ex}} (u_{m-1}^{k+1}) + \phi_{\text{im}} (u_{m-1}^{k+1}, u_{m}^{k+1}, t_{m}, \Delta t_{m}) \right] - \Delta t_{m} \left[\phi_{\text{ex}} (u_{m-1}^{k}) + \phi_{\text{im}} (u_{m-1}^{k}, u_{m}^{k}, t_{m}, \Delta t_{m}) \right]$$
(18)

for $m = 1, \dots M$.

Similarly, applying the two-stage first-order integrator (7) to (15) results in the SI1(2) corrector

$$\begin{split} \boldsymbol{u}^{(1)} &= \boldsymbol{u}_{m-1}^{k+1} + \boldsymbol{S}_{m}^{k} + \Delta t_{m} \big[\boldsymbol{\phi}_{\text{ex}} \big(\boldsymbol{u}_{m-1}^{k+1} \big) + \boldsymbol{\phi}_{\text{im}} \big(\boldsymbol{u}_{m-1}^{k+1}, \boldsymbol{u}^{(1)}, t_{m}, \Delta t_{m} \big) \big] \\ &- \Delta t_{m} \big[\boldsymbol{\phi}_{\text{ex}} \big(\boldsymbol{u}_{m-1}^{k} \big) + \boldsymbol{\phi}_{\text{im}} \big(\boldsymbol{u}_{m-1}^{k}, \boldsymbol{u}_{m}^{k}, t_{m}, \Delta t_{m} \big) \big] , \\ \boldsymbol{u}^{(2)} &= \boldsymbol{u}_{m-1}^{k+1} + \boldsymbol{S}_{m}^{k} + \Delta t_{m} \big[\boldsymbol{\phi}_{\text{ex}} \big(\boldsymbol{u}^{(1)} \big) + \boldsymbol{\phi}_{\text{im}} \big(\boldsymbol{u}_{m-1}^{k+1}, \boldsymbol{u}^{(2)}, t_{m}, \Delta t_{m} \big) \big] , \\ &- \Delta t_{m} \big[\boldsymbol{\phi}_{\text{ex}} \big(\boldsymbol{u}_{m}^{k} \big) + \boldsymbol{\phi}_{\text{im}} \big(\boldsymbol{u}_{m-1}^{k}, \boldsymbol{u}_{m}^{k}, t_{m}, \Delta t_{m} \big) \big] , \\ \boldsymbol{u}_{m}^{k+1} &= \boldsymbol{u}^{(2)} \end{split}$$

for m = 1, ... M.

Remark 2. Both correctors and thus the resulting SDC methods are semi-implicit, as the intermediate and final solutions appear only on the left-hand side and in ϕ_{im} .

It should be noted that a similar corrector can be derived from SI2(2). However, this approach would require additional data in the subinterval midpoints and would not promise faster convergence with non-equidistant collocation points [13]. Therefore, the present study focuses on SDC methods using first-order predictors and correctors. For concise notation, these methods are labeled SDC-SI(s_1,s_2) $_M^K$, where s_1 specifies the number of predictor stages, s_2 the number of corrector stages, s_2 the number of corrector stages, s_3 the number of collocation points and s_3 the total number of iterations, i.e. one predictor sweep and s_3 corrector sweeps.

Remark 3. When applying the integrators SI1(1) or SI1(2) as a predictor, they sweep through all subintervals one after the other. As a result the step size Δt is replaced by the subinterval length Δt_m in (6) and (7), respectively. Note that θ simultaneously assumes the same value, as it is fixed to the step size.

3.2.2. Equivalence to Radau IIA collocation and discontinuous Galerkin methods. If the SDC method converges, the difference between \boldsymbol{u}_m^k , \boldsymbol{u}_m^{k+1} and \boldsymbol{u}_m vanishes for $k \to \infty$. As a consequence, the solution satisfies the collocation scheme

$$\mathbf{u}_{m} = \mathbf{u}_{m-1} + \Delta t \sum_{i=1}^{M} w_{i,m} \mathbf{f}(\mathbf{u}_{i}, t_{i}), \quad m = 1, \dots M.$$
 (19)

By transforming (19) into a non-incremental form it can be shown that the scheme is identical to the Radau IIA collocation method of the order 2M-1

$$\mathbf{u}_{m} = \mathbf{u}(t_{0}) + \Delta t \sum_{n=1}^{M} a_{m,n} \mathbf{f}(\mathbf{u}_{n}, t_{0} + c_{n} \Delta t), \quad m = 1, ... M$$
 (20)

with the nodes $c_n = \tau_n$ and coefficients

$$a_{m,n} = \sum_{k=1}^{m} w_{n,k} = \int_0^{\tau_m} \ell_n(\tau) d\tau,$$

see Deuflhard and Bornemann [16, Ch. 6]. It is therefore expected that the corresponding SDC method will achieve the same order. Furthermore, it was proven in [36] that the Radau IIa method and thus the SDC method is equivalent to a discontinuous Galerkin method using the basis functions (13).

- **3.2.3.** Extension to other point sets and relation to Euler-based SDC methods. Similar SDC methods can be constructed using other sets of collocation points, e.g., Gauss, Gauss-Lobatto or equidistant points. The latter two include the left interval boundary, which must be taken into account when constructing the Lagrange interpolant $L(\underline{u},t)$. In addition, the first coefficient is then determined by the initial condition. Furthermore, it is noted that the one-step corrector (18) reproduces the Euler-based semi-implicit SDC method proposed by Minion [52] when $\theta=0$ is enforced in $\phi_{\rm im}$. This method was shown to increase the order of the approximate solution by one with each correction sweep, until the order of the underlying collocation method is reached [11, 27, 30]. In the following, the method is referred to as SDC-EU and used for comparison. Due to the similarity between SDC-EU and SDC-SI, it is assumed that both methods converge at the same rate.
- **3.2.4.** Linear stability of SDC methods. The Gauss-type collocation methods are known to be A-stable and the Radau IIA method is even L-stable [28]. Unfortunately, corresponding SDC methods do not necessarily inherit these properties. Even using backward Euler for prediction and correction is not sufficient to achieve A-stability [18]. Nevertheless, stable semi-implicit SDC methods can be constructed using the correctors proposed above.

Although the stability function of an SDC method is difficult to determine explicitly, it can be evaluated numerically by executing one time step of size $\Delta t = 1$ for the Dahlquist equation (9) with the initial condition $\hat{u}(0) = 1$. For comparison, Figure 3a shows the stability domains of the Euler-based semi-implicit SDC methods using M=2 to 8 Radau points and K=2M-1 iterations. The slope of the neutral stability curves suggests that these methods are $A(\alpha)$ -stable with α between 18° and 40°. In the case of pure convection, stability requires $z_i \lesssim M/2$, which is disappointing when compared with IMEX Runge-Kutta methods [2, 12]. Using the SI1(1) integrator for prediction and correction improves the stability considerably (Fig. 3b). The third-order method with two Radau points is even L-stable within the scope of numerical accuracy. This property is lost with increasing M, however the methods remain $A(\alpha)$ -stable with α between 40° and 80° and the convective stability limit doubles to $z_i \lesssim M$. The SDC methods, which are based on the twostage integrator SI1(2), achieve a further improvement and even appear A-stable at first glance (Fig. 3c). However, the zoom in Fig. 3d reveals unstable regions near the imaginary axis. A further improvement of stability was achieved by combining different predictors and correctors and adjusting the number of iterations. The resulting parameters are given in Tab. 1. Figure 3e shows the corresponding stability domains and Fig. 3f a close-up near the imaginary axis. Detailed numerical studies suggest that the improved methods are L-stable up to order 11 or 6 Radau points. The methods with 7 and 8 points are not A-stable, but instability is observed only in small regions close to the imaginary axis, see Tab. 1.

4. Spatial discretization

4.1. Preliminaries. The time integration methods developed in the previous section can be combined with any spatial discretization method. In the following, the discontinuous Galerkin method with nodal basis functions is used [33]. Subdividing Ω into non-overlapping elements Ω^e yields the computational domain $\Omega_h = \cup \Omega^e$ and the related set of element boundaries Γ_h . For a given time t, the approximate solution $u_h(x,t)$ is sought in the function space

$$\mathbb{U}_h = \left\{ \textbf{\textit{u}}_h \in \left[\mathbb{L}^2(\Omega) \right]^d \ : \ \textbf{\textit{u}}_h \big|_{\Omega^e} \in \left[\mathbb{P}_P(\Omega^e) \right]^d \quad \forall \Omega^e \in \Omega \right\},$$

where \mathbb{L}^2 is the space of square-integrable functions and \mathbb{P}_P the space of polynomials with degree less than or equal to P. The test space \mathbb{W}_h is mathematically identical to \mathbb{U}_h , but has reciprocal

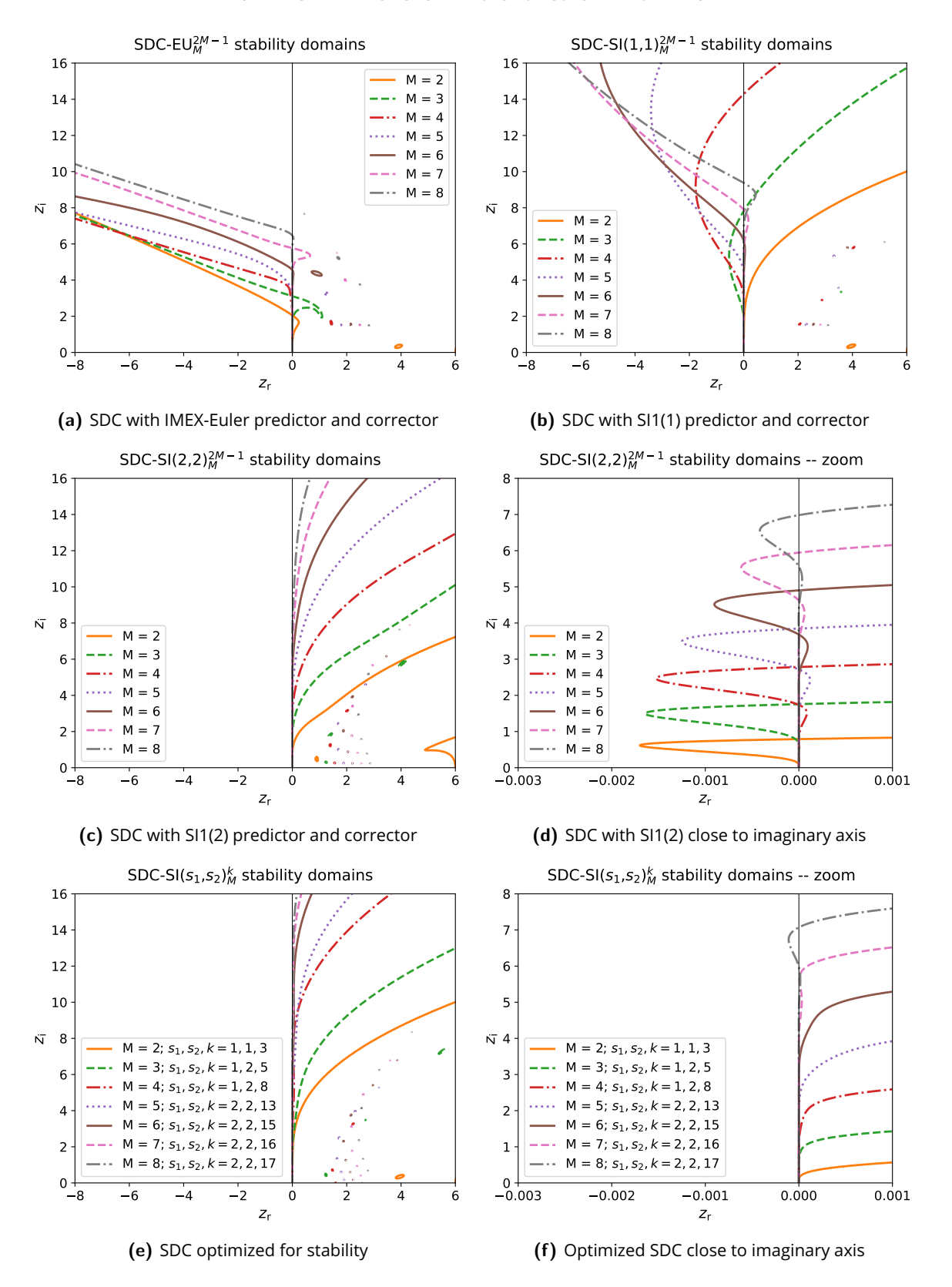


Figure 3. Neutral stability curves for SDC methods with up to M = 8 Radau points using different predictors and correctors

order	M	s_1	s_2	k	$z_{r,\max}$	
3	2	1	1	3	0	
5	3	1	2	5	0	
7	4	1	2	8	0	
9	5	2	2	13	0	
11	6	2	2	15	0	
13	7	2	2	16	-5.2e-7	
15	8	2	2	17	−1.1e−4	

Table 1. SDC-SI $(s_1,s_2)_M^k$ methods with optimal stability properties. The first column indicates the order of the underlying Gauss-Radau IIA method, M is the number of collocation points, s_1 the number of predictor stages, s_2 the number of corrector stages, k the total number of iterations and $z_{r,\max}$ the largest value on the real axis, so that the method is stable for all z_i .

physical dimensions, so that the product $\boldsymbol{w}_h^{\mathrm{t}}\boldsymbol{u}_h$ is well-defined for any $\boldsymbol{w}_h \in \mathbb{W}_h$. Finally, the average and jump operators on the joint boundary between elements Ω^- and Ω^+ are defined by

$$\{ u_h \} = \frac{u_h^- + u_h^+}{2},$$
$$[u_h] = n^- u_h^- + n^+ u_h^+,$$

where u_h^{\pm} are the traces of the corresponding element solutions and n^{\pm} the normals.

4.2. Discontinuous Galerkin formulation. Terms with no spatial derivatives are discretized using the projection operator

$$\mathcal{M}(\boldsymbol{w}_h, \boldsymbol{u}_h) = \int_{\Omega_h} \boldsymbol{w}_h^{\mathsf{t}} \boldsymbol{u}_h \, \mathrm{d}x \,. \tag{21}$$

In particular, the source term becomes

$$\mathcal{F}_{s}(\boldsymbol{w}_{h}, \boldsymbol{u}_{h}, t) = \mathcal{M}(\boldsymbol{w}_{h}, \boldsymbol{f}_{s}(\boldsymbol{u}_{h}, x, t)).$$

The convection term is discretized as

$$\mathcal{F}_{c}(\boldsymbol{w}_{h}, \boldsymbol{u}_{h}) = \int_{\Omega_{h}} (\partial_{x} \boldsymbol{w}_{h})^{t} \boldsymbol{f}_{c}(\boldsymbol{u}_{h}) dx + \sum_{\Gamma_{h}} [[\boldsymbol{w}_{h}]]^{t} \widehat{\boldsymbol{f}}_{c}(\boldsymbol{u}_{h}), \qquad (22)$$

where $\hat{f}_{\rm c}$ is the Riemann flux in the scalar case and the Roe flux with sonic fix of Harten and Hyman [31] in the Euler or Navier-Stokes case. Applying the symmetric interior penalty method to diffusion terms results in

$$\mathcal{F}_{d}(\boldsymbol{w}_{h}, \boldsymbol{u}_{h}, \boldsymbol{A}_{h}) = -\int_{\Omega_{h}} \partial_{x} \boldsymbol{w}_{h}^{t} \boldsymbol{A}_{h} \partial_{x} \boldsymbol{u}_{h} \, dx$$

$$+ \sum_{\Gamma_{h}} \left(\left\{ \left[\boldsymbol{A}_{h}^{t} \partial_{x} \boldsymbol{w}_{h} \right] \right\} \left[\left[\boldsymbol{u}_{h} \right] \right] + \left[\left[\boldsymbol{w}_{h} \right] \right] \left\{ \left[\boldsymbol{A}_{h} \partial_{x} \boldsymbol{u}_{h} \right] \right\} \right)$$

$$- \sum_{\Gamma_{h}} \mu \left[\left[\boldsymbol{w}_{h} \right] \right] \hat{\boldsymbol{A}} \left[\left[\boldsymbol{u}_{h} \right] \right] , \qquad (23)$$

where $m{A}_h$ is the diffusion matrix, $\hat{m{A}}$ the interface diffusion matrix with components

$$\widehat{A}_{i,j} = \begin{cases} \max(A_{i,j}^-, A_{i,j}^+) & i = j \\ \frac{1}{2}(A_{i,j}^- + A_{i,j}^+) & i \neq j \end{cases}$$

and

$$\mu = c_{\mu} \left\{ \left[\frac{P(P+1)}{2\Delta x^{e}} \right] \right\} \tag{24}$$

the penalty factor with the element width Δx^e and $c_{\mu} >$ 1, see e.g. [65].

Remark 4. The numerical fluxes introduced in the convection and diffusion terms are unique at the boundaries between the elements and thus preserve the conservation properties. This can illustrated by choosing $\boldsymbol{w}_h = \boldsymbol{1}$ which eliminates all boundary contributions in (22) and (23).

4.3. Shock capturing. Following Persson and Peraire [56], an artificial diffusivity $v_{\rm s}$ is introduced to capture unresolved discontinuities. The diffusivity is constant in each element and applies to all conservation variables. It can be included by adding a diagonal entry to the diffusion matrix, so that $f_{\rm d} = (A_{\rm d} + v_{\rm s} {\bf I}) \, \partial_x {\bf u}$. The method is briefly described to define the parameters:

First select a quantity of interest q and determine its Legendre expansion

$$q^e = \sum_{i=0}^P q_i^e L_i$$

in element Ω^e . Define the filtered quantity

$$\tilde{q}^e = \sum_{i=0}^{P-1} q_i^e L_i$$

and evaluate the smoothness indicator

$$s^e = \log_{10} \left(\frac{\|q^e - \tilde{q}^e\|_2^2}{\|q^e\|_2^2} \right),$$

where $\|\cdot\|$ is the L^2 norm on Ω^e . Then define the artificial diffusivity in Ω^e by

$$v_{s}^{e} = \begin{cases} 0 & \text{if } s_{0} - \kappa_{s} > s^{e}, \\ \hat{v}_{s}^{e} \frac{1}{2} \left(1 + \sin \frac{\pi(s^{e} - s_{0})}{2\kappa_{s}} \right) & \text{if } s_{0} - \kappa_{s} \leq s^{e} \leq s_{0} + \kappa_{s}, \\ \hat{v}_{s}^{e} & \text{if } s_{0} + \kappa_{s} < s^{e}, \end{cases}$$
(25)

where s_0 is a reference value, κ_s is the half width of the activation interval,

$$\hat{v}_{\rm s}^e = c_{\rm s} \lambda_{\rm c,max}^e \frac{\Delta x^e}{P}$$

the maximum diffusivity, $c_{\rm s}$ a scaling factor and $\lambda_{\rm c,max}^e$ the maximum magnitude of the eigenvalues of ${\bf A}_{\rm c}$ in Ω^e . In the studies presented below, q=u was chosen for the Burgers equation and $q=\rho$ for the Euler equations. The reference value is fixed to $s_0=-4(\log_{10}P+1)$, while $c_{\rm s}$ and $\kappa_{\rm s}$ are adapted to each test case. It should be noted that several improvements to the method have been proposed, but these are beyond the scope of this paper, see e.g. [4, 22, 45].

4.4. Application to time integration methods. In the course of spatial discretization, the RHS functions introduced in Sec. 3 are replaced by the functionals

$$\begin{split} \boldsymbol{\Phi}_{\mathrm{ex}} \left(\boldsymbol{w}_{h}, \boldsymbol{u}_{h}^{\alpha} \right) &= \mathcal{F}_{\mathrm{c}} \left(\boldsymbol{w}_{h}, \boldsymbol{u}_{h}^{\alpha} \right), \\ \boldsymbol{\Phi}_{\mathrm{im}} \left(\boldsymbol{w}_{h}, \boldsymbol{u}_{h}^{\alpha}, \boldsymbol{u}_{h}^{\beta}, t, \theta \right) &= \mathcal{F}_{\mathrm{d}} \left(\boldsymbol{w}_{h}, \boldsymbol{u}_{h}^{\beta}, \frac{\theta}{2} \boldsymbol{A}_{\mathrm{c}}^{2} (\boldsymbol{u}_{h}^{\alpha}) + \boldsymbol{A}_{\mathrm{d}} (\boldsymbol{u}_{h}^{\alpha}) + \boldsymbol{v}_{s} (\boldsymbol{u}_{h}^{\alpha}) \mathbf{I} \right) + \mathcal{F}_{\mathrm{s}} \left(\boldsymbol{w}_{h}, \boldsymbol{u}_{h}^{\alpha}, t \right), \\ \mathcal{F} \left(\boldsymbol{w}_{h}, \boldsymbol{u}_{h}^{\alpha}, t \right) &= \mathcal{F}_{\mathrm{c}} \left(\boldsymbol{w}_{h}, \boldsymbol{u}_{h}^{\alpha} \right) + \mathcal{F}_{\mathrm{d}} \left(\boldsymbol{w}_{h}, \boldsymbol{u}_{h}^{\alpha}, \boldsymbol{A}_{\mathrm{d}} (\boldsymbol{u}_{h}^{\alpha}) + \boldsymbol{v}_{s} (\boldsymbol{u}_{h}^{\alpha}) \mathbf{I} \right) + \mathcal{F}_{\mathrm{s}} \left(\boldsymbol{w}_{h}, \boldsymbol{u}_{h}^{\alpha}, t \right). \end{split}$$

As a result, the SI1(1) integrator (6) takes form

$$\mathcal{M}(\boldsymbol{w}_h, \boldsymbol{u}_h^{n+1}) = \mathcal{M}(\boldsymbol{w}_h, \boldsymbol{u}_h^n) + \Delta t \left[\boldsymbol{\Phi}_{\text{ex}}(\boldsymbol{w}_h, \boldsymbol{u}_h^n) + \boldsymbol{\Phi}_{\text{im}}(\boldsymbol{w}_h, \boldsymbol{u}_h^n, \boldsymbol{u}_h^{n+1}, t^{n+1}, \Delta t) \right]$$

and the SI1(1) corrector (18) becomes

$$\begin{split} \mathcal{M}(\boldsymbol{w}_h, \boldsymbol{u}_{h,m}^{k+1}) &= \mathcal{M}(\boldsymbol{w}_h, \boldsymbol{u}_{h,m-1}^{k+1}) + \mathcal{S}_{h,m}^k \\ &+ \Delta t_m \big[\boldsymbol{\Phi}_{\mathrm{ex}} \big(\boldsymbol{w}_h, \boldsymbol{u}_{h,m-1}^{k+1} \big) + \boldsymbol{\Phi}_{\mathrm{im}} \big(\boldsymbol{w}_h, \boldsymbol{u}_{h,m-1}^{k+1}, \boldsymbol{u}_{h,m}^{k+1}, t_m, \Delta t_m \big) \big] \\ &- \Delta t_m \big[\boldsymbol{\Phi}_{\mathrm{ex}} \big(\boldsymbol{w}_h, \boldsymbol{u}_{h,m-1}^k \big) + \boldsymbol{\Phi}_{\mathrm{im}} \big(\boldsymbol{w}_h, \boldsymbol{u}_{h,m-1}^k, \boldsymbol{u}_{h,m}^k, t_m, \Delta t_m \big) \big] \end{split}$$

with

$$S_{h,m}^k = \mathcal{M}(\boldsymbol{w}_h, \boldsymbol{S}_m^k) = \Delta t \sum_{i=1}^M w_{i,m} \mathcal{F}(\boldsymbol{w}_h, \boldsymbol{u}_{h,i}^k, t_i).$$

The application to the two-stage methods proceeds analogously. Finally, the discrete form of the collocation method (20) reads

$$\mathcal{M}(\boldsymbol{w}_h, \boldsymbol{u}_{h,m}) = \mathcal{M}(\boldsymbol{w}_h, \boldsymbol{u}_h(t_0)) + \Delta t \sum_{n=1}^{M} a_{m,n} \mathcal{F}(\boldsymbol{w}_h, \boldsymbol{u}_{h,n}, t_0 + c_n \Delta t), \quad m = 1, \dots M.$$
 (26)

Remark 5. Equation (26) corresponds to a space-time discontinuous Galerkin formulation due to the equivalence between Radau IIA and DG in time.

Remark 6. The collocation method and the SDC methods presented above are conservative, as they are linear combinations of the conservative building blocks $\Phi_{\rm ex}$ and $\Phi_{\rm im}$.

5. Solution techniques

- **5.1. Numerical integration.** The integrals in the spatial operators are evaluated using a Gauss-Lobatto quadrature with Q+1 points. For the convection term Q is chosen large enough to avoid aliasing errors caused by nonlinearities. In the numerical experiments reported below, Q=P is used for the convection-diffusion equation, $Q=\lceil 3P/2 \rceil$ for the Burgers equation and Q=2P for the Euler and Navier-Stokes equations. The remaining terms are integrated with Q=P so that the quadrature points coincide with the spatial collocation points and therefore no interpolation is necessary. This approach leads to a diagonal mass matrix, which simplifies the evaluation and inversion of the projection operator (21).
- **5.2. Solution of implicit equations.** The spatio-temporal discretization leads to linear systems of equations that can be written symbolically in the form

$$Ku = b$$
,

where \underline{u} is the solution vector, \underline{K} a positive definite matrix and \underline{b} the RHS. Systems of this type can be solved very efficiently with tailored multigrid methods [38, 49, 64, 65], but these are beyond the scope of the present study. Instead, a preconditioned conjugate gradient method is used for scalar cases and the FGMRES method in the Euler and Navier-Stokes cases [23, 32, 59]. Additionally, a

fast direct solver was developed for the convection diffusion equation with constant diffusion matrices $\boldsymbol{A}_{\rm d}$ and $\boldsymbol{A}_{\rm c}$. This solver is used in performance tests to demonstrate the competitiveness of the proposed SDC methods.

6. Numerical Experiments

The accuracy and stability of the newly developed SDC-SI methods are evaluated by means of numerical experiments for linear convection-diffusion, Burgers and compressible flow problems. For comparison with the linear stability analysis in Sec. 3, the CFL number is defined as

$$CFL = \frac{\Delta t \, \lambda_{c,\text{max}}}{\Delta x} \,,$$

where Δx is a length scale characterizing the mesh spacing. Following the analysis in [10, Sec. 7.3.3], the length scale is chosen as

$$\Delta x = \frac{\Delta x^e}{2\delta} \,,$$

where $\delta \sim P^2$ is the largest eigenvalue of the convection problem with unit velocity and one-sided Dirichlet conditions in the standard element [-1,1]. Unless stated otherwise, the CFL number is determined from the initial conditions. The IMEX Euler-based SDC-EU method, the second-order IMEX-RK CB2 Runge-Kutta method of Cavaglieri and Bewley [12], the third order explicit TVD-RK3 method of Shu and Osher [60] and the third order ARS(4,4,3) method of Ascher et al. [2] are used for comparison.

6.1. Convection-diffusion equation. The first set of test problems relates to the convection-diffusion equation (2) with the exact solution given by

$$u(x,t) = \sum_{i=1}^{7} a_i \sin\left(\kappa_i(x - s_i - vt)\right) e^{-\kappa_i^2 vt}$$
(27)

and v=1. Equation (27) defines a wave packet including a variety of wave numbers κ_i , amplitudes a_i and phase shifts s_i that are specified in Tab. 2. The tests are performed in the periodic domain $\Omega=[0,1]$ using 64 elements of degree 15. This resolution is fine enough to neglect spatial discretization errors.

The first test considers the case of pure convection in the time interval [0, 10], i.e. ten periods of the longest wave. Starting from 64, the CFL number is successively reduced by a factor of 2 down to 1/256. Figure 4a shows the L^2 error at the final time for selected standalone integrators. Due to the absence of diffusivity, SI1(1) and SI2(2) produce virtually identical results. They are stable over the entire range and converge at a rate of approximately Δt^2 for CFL numbers below 2. The second-order IMEX-RK CB2 is less accurate and only succeeds at CFL < 1/16 when the numerical diffusion introduced by the Riemann fluxes is large enough to stabilize the method. IMEX-RK ARS(4,4,3) and TVD-RK3 achieve their theoretical order of 3 and are the most accurate of the standalone integrators tested. Note that TVD-RK3 remained stable up to $CFL \approx 0.87$, which is close to the theoretical threshold of 1 and thus confirms the chosen definition of the CFL number. Figure 4b shows the corresponding results for the Euler based SDC methods with M=2 to 8 Radau points and 2M-1 iterations in every time step. With M=2 or M=3 the method achieves the expected convergence rate of 2M-1. Increasing the number of collocation points improves the accuracy rapidly, while the stability threshold rises slowly from CFL = 1/2 to 2. In contrast, the SDC-SI method with up to 8 Radau points and s_1 , s_2 stages according to Tab. 1 proved stable over the entire CFL range (Fig. 4c). With M=2 to 4 points the method achieves the expected order of

i	1	2	3	4	5	6	7
κ_i	2π	6π	10π	14π	18π	24π	30π
a_i	1.00	1.50	1.80	1.70	1.50	1.30	1.15
S_i	0.00	0.05	0.10	0.15	0.20	0.30	0.18

Table 2. Wave packet coefficients

2M-1. For larger M the convergence rate cannot be estimated due to the missing asymptotic range (Fig. 4d).

The second test assumes a diffusivity of $\nu = 0.001$. Figure 4e shows a faster convergence in this case, which can be attributed to the damping of the short-wave components and the simpler solution structure at the end time. The experimental order of convergence, on the other hand, changes only slightly (Fig. 4f).

6.2. Burgers equation. The Burgers equation poses a challenge to numerical methods as it allows for nonlinear interactions, including the formation of discontinuities. Furthermore, the resulting variation of the convective Jacobian matrix leads to a variable diffusivity in the semi-implicit methods developed in this work.

The first test case examines the wave packet (27) with the parameters given in Tab. 2. In order to satisfy the Burgers equation, the source term is defined as

$$f_{\rm s}(x,t) = \partial_t u + \partial_x \left(\tfrac{1}{2} u^2 \right) - \partial_x (v \partial_x u) \,,$$

based on the exact solution u(x,t). The computational domain and the discretization parameters are identical to the convection-diffusion problem above. As an example, Figure 5 shows the results obtained with the SDC-SI method for v=0. Despite the nonlinearity of the Burgers equation, the method proved to be robust and succeeded in all cases with CFL numbers of at least 32. The observed errors and convergence rates agree well with the corresponding results for the convection-diffusion problem in Fig. 4c,d.

The next test case relates to the moving front solution

$$u(x,t) = 1 - \tanh\left(\frac{x + 0.5 - t}{2\nu}\right)$$

for $x \in [-1,1]$, see [33]. Assuming a diffusivity of v=0.001 yields a thin front advancing with unit velocity. Two scenarios are considered: the first one uses 50 elements of degree 15 and the second 20 elements of degree 10. Time integration is performed over the interval [0,0.5] with N_t steps. The first scenario is characterized by a marginal spatial resolution, which is sufficient to capture the front with an L^2 error of about 6×10^{-4} . Figure 6a shows the corresponding convergence results for the Euler based SDC-EU method as a basis for comparison. Note that the method achieves optimal accuracy with $CFL \le 4$, but fails with larger steps. In contrast, the SDC-SI method succeeds for all M with only $N_t=16$ steps or $CFL\approx 64$ (Fig. 6b). As the CFL number decreases, the method converges and reaches the minimal error with half as many steps as SDC-EU. Figure 6c shows the behavior of the solution obtained with SDC-SI(2,2) $_6^{11}$ for different CFL numbers. Although spurious oscillations occur, the method remains stable up to CFL=64. The inset gives a close view on the upstream region near the front and illustrates how the oscillations reduce as the time step decreases. At $CFL \le 16$ the minimum error is reached and leaves slight ripples due to the marginal spatial resolution.

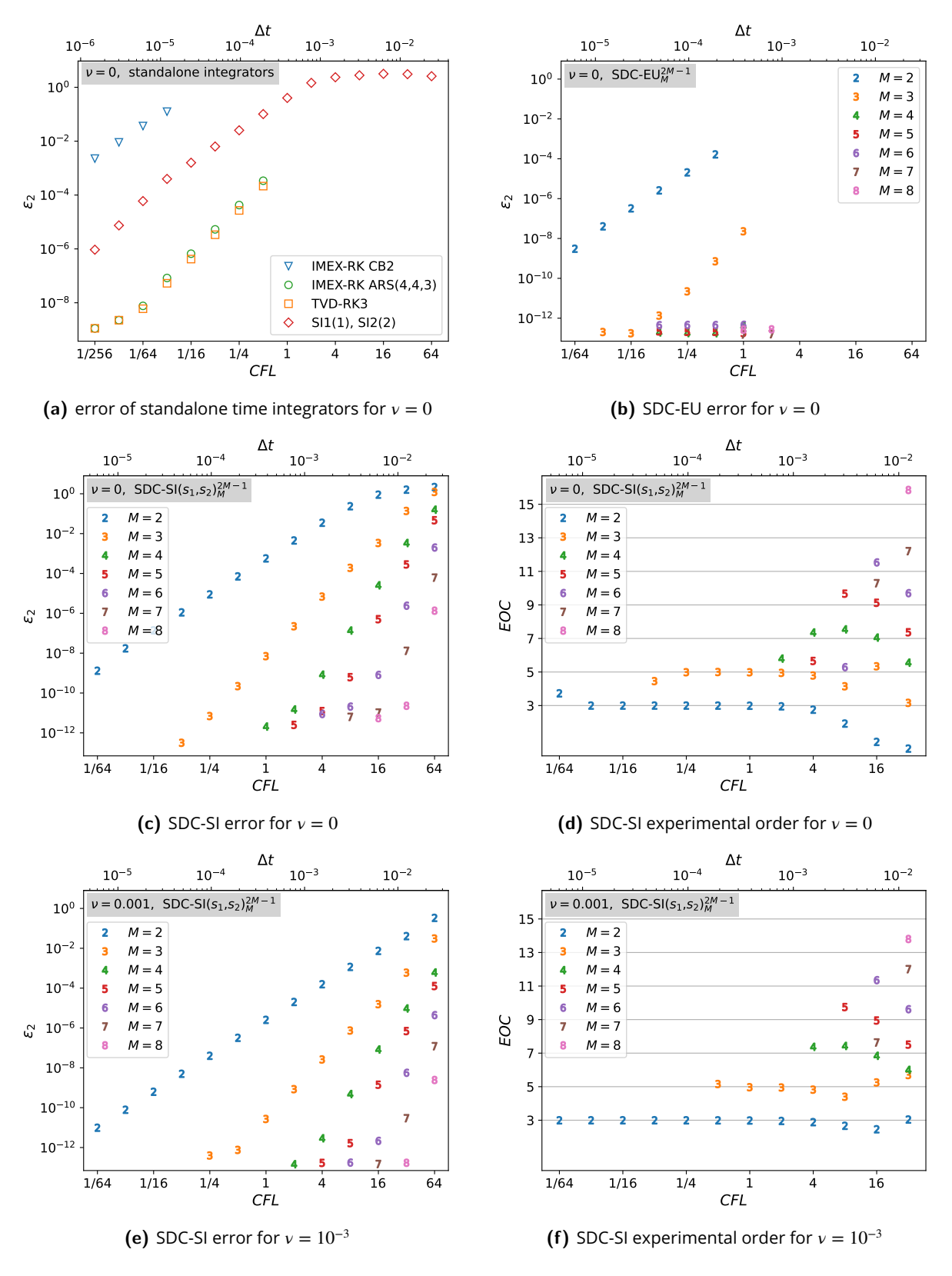


Figure 4. Convergence study for the convection-diffusion wave problem.

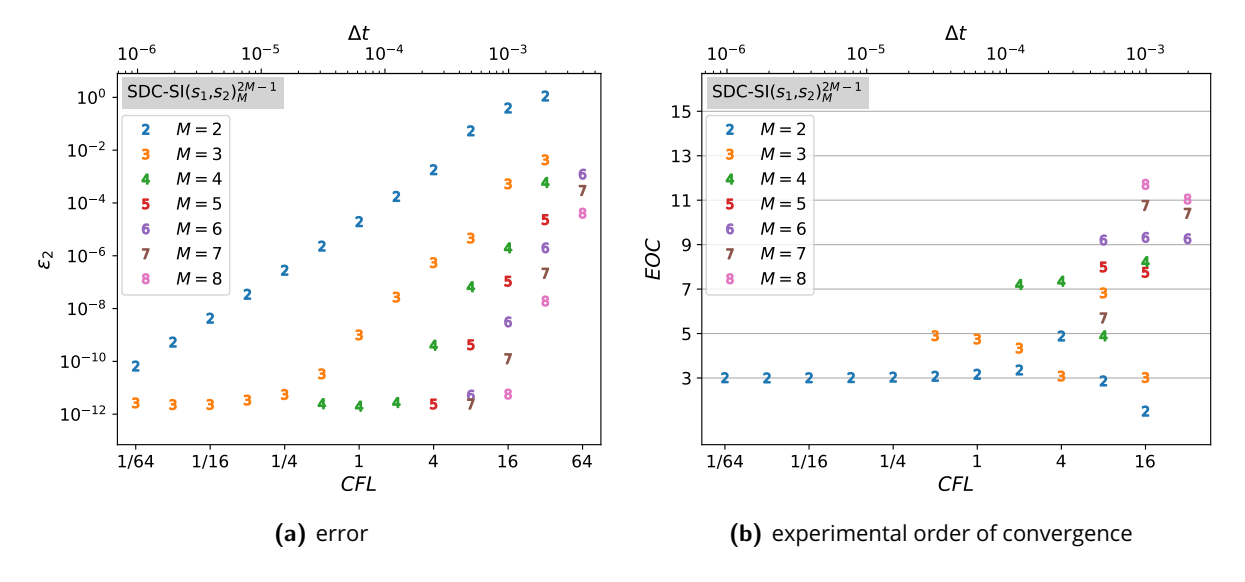


Figure 5. Convergence of the SDC-SI method for the inviscid Burgers wave problem

In the second scenario the artificial diffusivity (25) is used with parameters $\kappa_{\rm s}=2$ and $c_{\rm s}=0.4$. Figure 6d shows the numerical solution obtained with SDC-SI(2,2) $_6^{11}$ for selected step numbers N_t . The method succeeds already with 4 steps, although with oscillations somewhat larger as depicted for $N_t=5$. As the number of steps increases, these oscillations disappear gradually and nearly vanish for $N_t=10$ or $CFL\approx20$. The solutions obtained with 20 and 40 steps are close to the temporally converged case and hence almost identical.

6.3. Euler and Navier-Stokes equations. The final series of tests deals with a selection of compressible flow problems. The fluid is a perfect gas with R=287.28 and $\gamma=1.4$, which corresponds to air when assuming SI units.

The first problem describes an acoustic wave traveling downstream in a uniform flow with Mach number Ma=0.1, pressure $p_{\infty}=1000$, temperature $T_{\infty}=300$, dynamic viscosity $\eta=10^{-5}$ and Prandtl number Pr=0.75. It is initialized by superimposing the periodic velocity perturbation

$$v'(x) = \hat{v}\sin(2\pi x)$$

with an amplitude of $\hat{v}=10^{-2}a_{\infty}$, where $a_{\infty}\approx 347.36$ is the speed of sound in the undisturbed fluid. Assuming an isotropic state, the initial temperature is given by

$$T_0(x) = \frac{1}{\gamma R} \left(a_{\infty} + \frac{\gamma - 1}{2} v' \right)^2,$$

the pressure by

$$p_0(x) = p_{\infty} \left(\frac{T}{T_{\infty}}\right)^{\gamma/(\gamma-1)}$$

and the velocity by

$$v_0(x) = Ma a_{\infty} + v'(x).$$

Note that the amplitude is large enough to expect a nonlinear steepening. In contrast, viscous damping is negligible due to the high Reynolds number $Re = \rho_{\infty} a_{\infty}/\eta \approx 4 \times 10^5$. The evolution of the wave is studied in the periodic domain $\Omega = [0,1]$ from t=0 to $t_{\rm end} = 2.619 \times 10^{-2}$, which

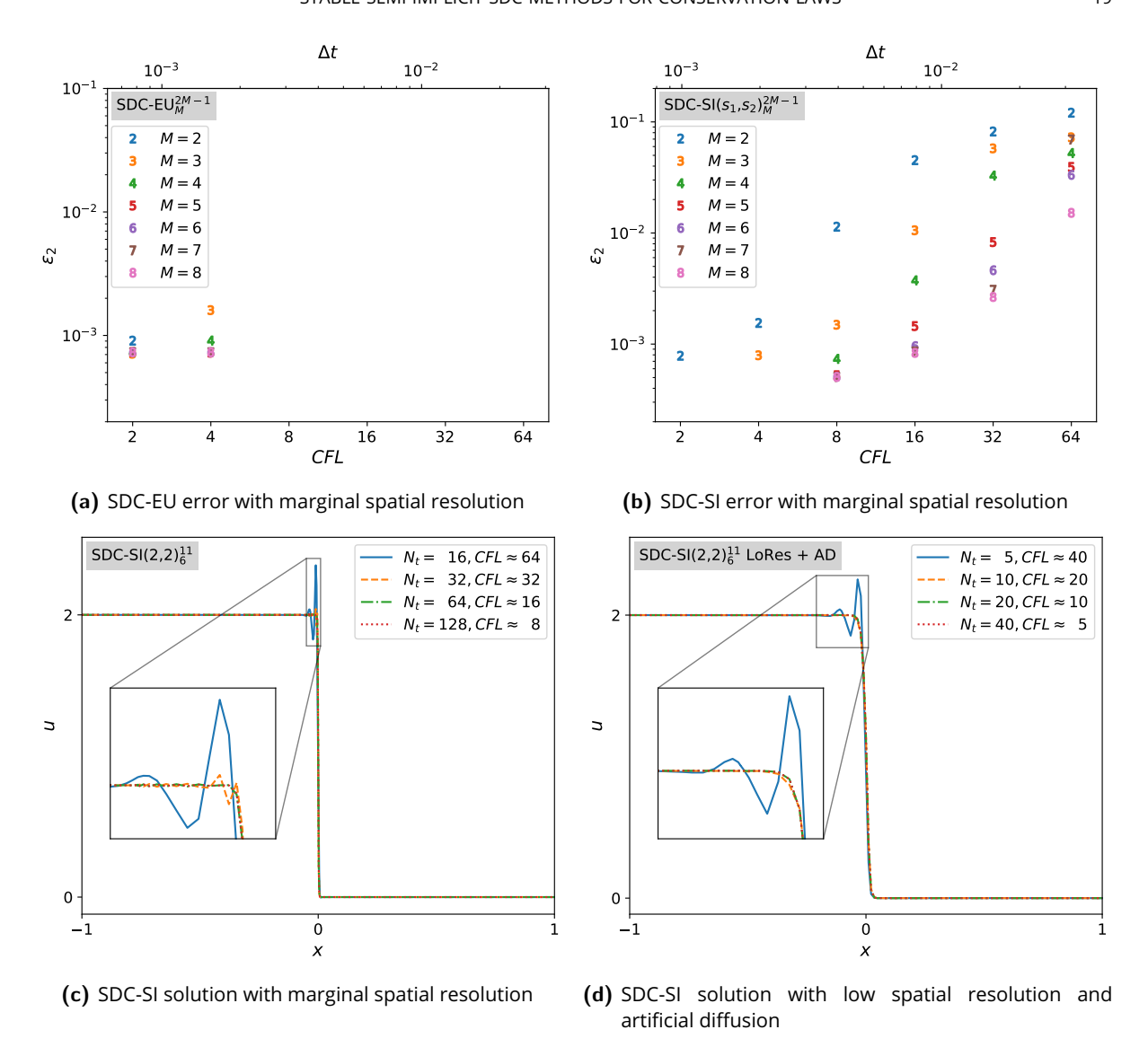


Figure 6. Results for the Burgers moving front problem

corresponds to approximately 10 convective units. For spatial discretization, the domain is decomposed into 10 elements of degree 15. Since no exact solution is available, the TVD-RK3 method with $\Delta t \approx 10^{-7}$ or $CFL \approx 0.016$ serves as a reference. The SDC-SI method was applied with M=2 to 8 Radau points and 2M-1 iterations. Between $N_t=4$ and 64, 826 time steps were used for time integration, which corresponds to CFL numbers in the range from 1/32 to 1013. The fact that all runs were successful underlines the stability of the method. As an example, the computed density distributions are shown in Fig. 7a for M=3 and in Fig. 7b for M=8. Note that the results are visually indistinguishable from the reference for $CFL\approx 16$ in the first case and $CFL\approx 64$ in the second case. Hence, only about 6 time steps with 8 subintervals are required for one convective unit.

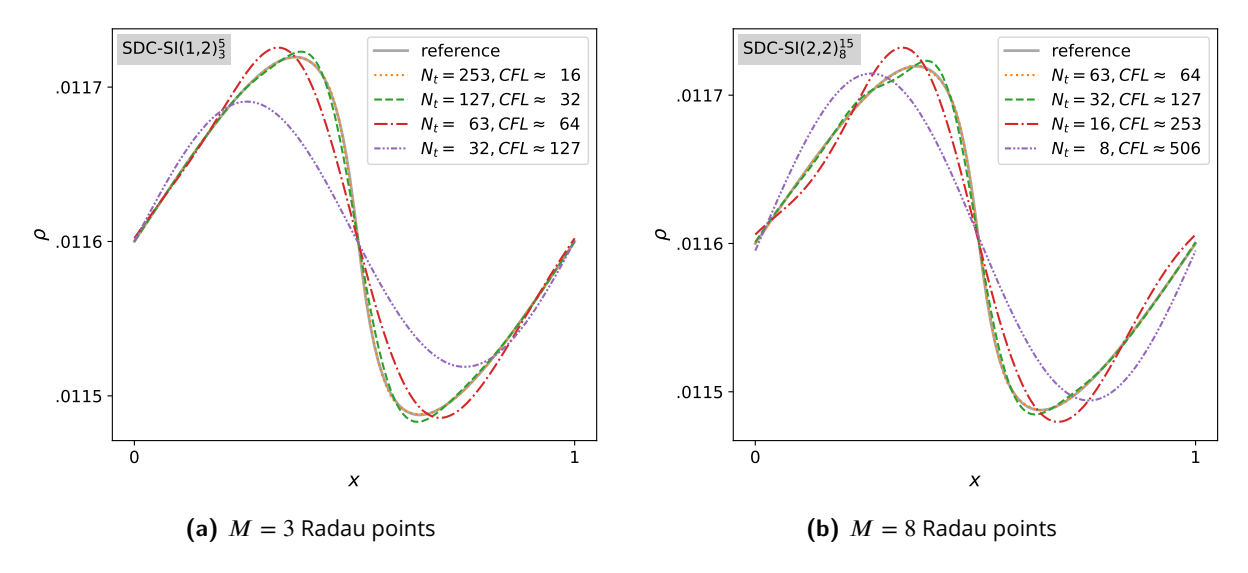


Figure 7. Acoustic wave density distributions obtained with SDC-SI(s_1, s_2) $_M^{2M-1}$

The second example is Sod's shock tube problem for the Euler equations with initial conditions [62]

$$\rho = 1,$$
 $p = 1,$ $v = 0$ if $x < 0.5$
 $\rho = 0.125,$ $p = 0.1,$ $v = 0$ if $x \ge 0.5$

to solve on $\Omega=[0,1]$ until t=0.2. For the numerical studies, the domain is divided into 80 elements of degree 5. The artificial diffusivity (25) is used with $\kappa_{\rm S}=6$ and $c_{\rm S}=0.4$ to capture the evolving shock and the contact discontinuity. Figure 8 shows the density and velocity distributions obtained with SDC-SI(2,2) $_6^{11}$ at different step sizes. TVD-RK3 with 10^5 steps or $\Delta t=2\times10^{-6}$ serves as a reference. Note that the SDC-SI method produces reasonable results with only 4 steps. This is remarkable, because the shock wave traverses a quarter of the domain during this time. Although the density and velocity distributions behind the shock show considerable oscillations, these decrease as the number of steps increases. With $N_t=32$ or $CFL\approx7$ they disappear and the solution is visually identical to the reference.

The final test case is the shock-fluctuation benchmark of Shu and Osher [61, Example 8] for the Euler equations with initial conditions

$$\rho = 3.857143$$
, $p = 10.33333$, $v = 2.629369$ if $x < -4$, $\rho = 1 + 0.2 \sin 5x$, $p = 1$, $v = 0$ if $x \ge -4$,

to solve on $\Omega=[-5,5]$ until t=1.8. This case is more challenging than Sod's problem as it involves the complex interaction between a strong discontinuity and smooth wave-like pattern. The numerical solutions were computed with 160 elements of degree 5 using the artificial diffusivity (25) for stabilization. Figure 9a shows the density distributions at t=1.8 for SDC-SI(2,2) $_6^{11}$ with varying temporal resolution and fixed stabilization parameters $\kappa_s=2$, $c_s=0.4$. The given CFL numbers were determined after $N_t/2$ steps. For $N_t \geq 400$ or $CFL \lesssim 2.3$ the results agree well with reference data obtained with TVD-RK3 using 180,000 steps or $\Delta t=1\times 10^{-5}$. With increasing step size, the error in the interaction zone behind the shock grows, but remains at a moderate level up to $N_t=100$ or $CFL\approx 9.3$. Using less than 90 steps leads to negative density or temperature

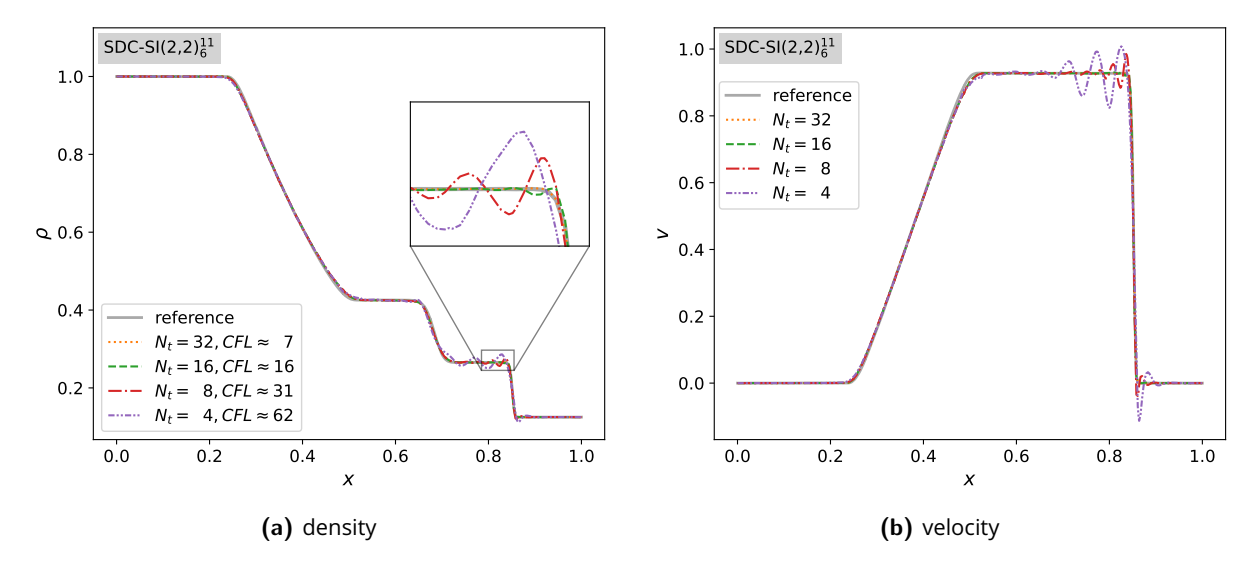


Figure 8. Shock tube results obtained with SDC-SI SDC-SI(2,2) $_6^{11}$ for different CFL numbers

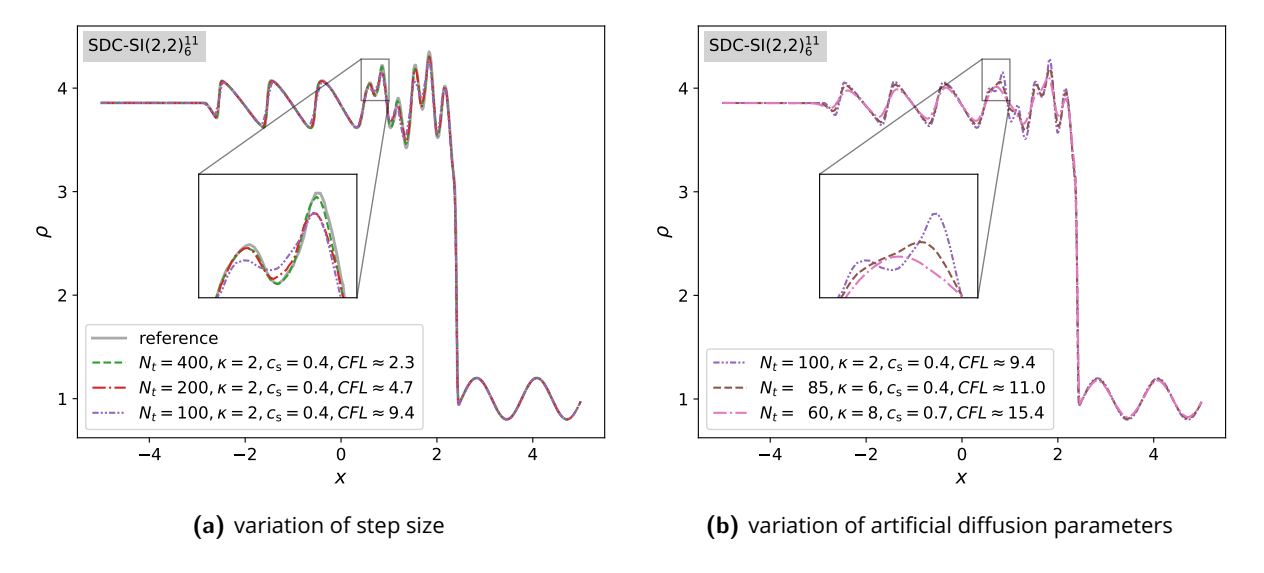


Figure 9. Shock-fluctuation interaction: density distributions obtained with SDC-SI(2,2) $_6^{11}$ for different step sizes (left) and different artificial diffusion parameters (right)

values in the intermediate solution and thus to failure of the method. In further tests, the SDC-SI method achieved CFL numbers between 8 with M=2 Radau points and 21 with M=16. A closer examination revealed that the resolution near the stability threshold is insufficient to capture the temporal development. As a consequence, the temporal interpolation leads to spurious oscillations which result in physically invalid intermediate values. In agreement with this observation, the stability threshold grows if the solution is smoothed by increasing the artificial diffusion. Figure 9b gives an example for SDC-SI(2,2) $_6^{11}$, where the use of a wider sensor interval and a higher maximum diffusivity increased the admissible step size by a factor of about 1.7.

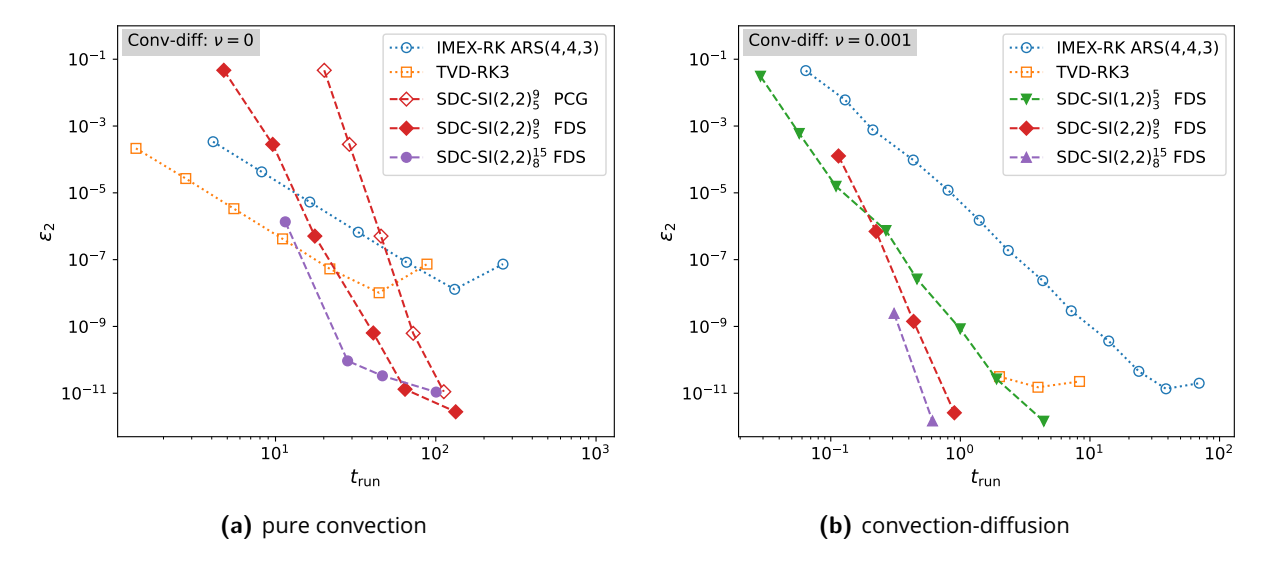


Figure 10. Error-runtime comparison between Runge-Kutta and SDC methods using either the preconditioned conjugate gradient method (PCG) or the fast direct solver (FDS)

6.4. Computational efficiency. In the numerical experiments described above, the focus was deliberately placed on stability and accuracy. The iteration counts and terminal conditions for solving the implicit equation systems were chosen carefully to exclude adverse effects due to algebraic errors. In addition, the iterative solvers have not yet been optimized and are therefore inferior to explicit methods such as TVD-RK3. However, to demonstrate the potential of the proposed SDC methods, performance tests were performed for the convection-diffusion equation for which a fast direct solver is available. Figure 10a shows a comparison between Runge-Kutta and SDC methods for the purely convective wave problem studied in Sec. 6.1. For errors down to 10^{-6} TVD-RK3 outperforms the other methods, which is not surprising because the method was designed for this type of problems. IMEX-RK ARS(4,4,3) requires about three times the time to achieve the same error. The SDC methods are more expensive in this error range, but become competitive with increasing accuracy, especially when using the fast solver. For example, the SDC-SI(2,2) method with 8 Radau points surpasses TVD-RK3 for errors below 10^{-6} . In presence of diffusion, the advantage of explicit Runge-Kutta methods diminishes further. As an example, Figure 10b shows the results for v = 0.001. Although convection still dominates, the SDC methods with 3, 5 or 8 Radau points clearly outperform the Runge-Kutta methods in the entire error range.

7. Conclusions

This work presents a new family of spectral deferred correction (SDC) methods with excellent stability properties. The key ingredient are novel time integrators which combine a semi-implicit splitting of the convection term inspired by the Lax-Wendroff method with an implicit treatment of diffusion and sources. These integrators possess excellent stability properties and require only the solution of positive definite or semi-definite linear systems. In the present study they were used to construct semi-implicit SDC methods on the basis of right-sided Radau points. Numerical evidence suggests that these methods are L-stable with 2 to 6 points or orders from 3 to 11 and require very little diffusion for orders 13 and 15.

In numerical experiments, the SDC methods were applied to high-order discontinuous Galerkin formulations of one-dimensional conservation laws. Tests with the convection-diffusion equation proved the excellent stability and accuracy of the methods: They remained stable with CFL numbers up to at least 64 and achieved the expected order of convergence, i.e. 2M-1 with M Radau points. In comparison, the SDC method based on the IMEX Euler scheme reached CFL numbers of only 0.5 with M=2 and 2 with $M\geq 4$. Excellent results were also obtained for nonlinear problems, including the Burgers, Euler and Navier-Stokes equations. In particular, it could be shown that the proposed SDC methods can handle marginally resolved solutions and easily accommodate artificial diffusion techniques for stabilization near discontinuities. Future work should focus on acceleration, e.g., by using multilevel techniques and generalization to multidimensional problems [63].

Data Availability

The datasets generated during the current study are available from the corresponding author on reasonable request.

Funding

Funding by German Research Foundation (DFG) in frame of the project STI 57/9-1 is gratefully acknowledged. The author would like to thank ZIH, TU Dresden, for the provided computational resources. Open Access funding is enabled and organized by Projekt DEAL.

Ethics declarations

The author declares that he has no known competing financial interests or personal relationships that could have appeared to influence the work reported in this paper.

References

- [1] U. M. Ascher, S. J. Ruuth, and B. T. R. Wetton. Implicit-explicit methods for time-dependent partial differential equations. *SIAM Journal on Numerical Analysis*, 32(3):797–823, 1995. doi: 10.1137/0732037.
- [2] U. M. Ascher, S. J. Ruuth, and R. J. Spiteri. Implicit-explicit Runge-Kutta methods for time-dependent partial differential equations. *Applied Numerical Mathematics*, 25(2-3):151–167, 1997. doi: 10.1016/s0168-9274(97)00056-1.
- [3] A. Baeza, R. Bürger, M. d. C. Martí, P. Mulet, and D. Zorío. On approximate implicit taylor methods for ordinary differential equations. *Computational and Applied Mathematics*, 39(4), 2020. doi: 10.1007/s40314-020-01356-8.
- [4] G. E. Barter and D. L. Darmofal. Shock capturing with pde-based artificial viscosity for dgfem: Part i. formulation. *Journal of Computational Physics*, 229(5):1810–1827, 2010. doi: 10.1016/j. jcp.2009.11.010.
- [5] F. Bassi, L. Botti, A. Colombo, A. Ghidoni, and F. Massa. Linearly implicit Rosenbrock-type Runge–Kutta schemes applied to the discontinuous Galerkin solution of compressible and incompressible unsteady flows. *Computers & Fluids*, 118:305–320, 2015. doi: $10.1016/\mathrm{j}$. compfluid.2015.06.007.
- [6] S. Boscarino, F. Filbet, and G. Russo. High order semi-implicit schemes for time dependent partial differential equations. *Journal of Scientific Computing*, 68(3):975–1001, 2016. doi: $10.1007/\mathrm{s}10915-016-0168-\mathrm{y}$.

- [7] W. Boscheri and M. Tavelli. High order semi-implicit schemes for viscous compressible flows in 3d. *Applied Mathematics and Computation*, 434:127457, 2022. doi: 10.1016/j.amc.2022. 127457.
- [8] A. N. Brooks and T. J. Hughes. Streamline upwind/petrov-galerkin formulations for convection dominated flows with particular emphasis on the incompressible navier-stokes equations. *Computer Methods in Applied Mechanics and Engineering*, 32(1–3):199–259, Sept. 1982. doi: 10.1016/0045-7825(82)90071-8.
- [9] C. Canuto, M. Y. Hussaini, A. Quarteroni, and T. A. Zang. Spectral Methods. Evolution to Complex Geometries and Applications to Fluid Dynamics. Springer-Verlag GmbH, 2007. ISBN 3540307273.
- [10] C. Canuto, M. Y. Hussaini, A. Quarteroni, and T. A. Zang. *Spectral Methods. Fundamentals in Single Domains*. Springer Berlin Heidelberg, 2011. ISBN 3540307257.
- [11] M. Causley and D. Seal. On the convergence of spectral deferred correction methods. *Communications in Applied Mathematics and Computational Science*, 14(1):33–64, 2019. doi: $10.2140/\mathrm{camcos}.2019.14.33$.
- [12] D. Cavaglieri and T. Bewley. Low-storage implicit/explicit Runge-Kutta schemes for the simulation of stiff high-dimensional ODE systems. *Journal of Computational Physics*, 286:172–193, 2015. doi: $10.1016/\mathrm{j.jcp.}2015.01.031$.
- [13] A. Christlieb, B. Ong, and J.-M. Qiu. Comments on high-order integrators embedded within integral deferred correction methods. *Communications in Applied Mathematics and Computational Science*, 4(1):27–56, 2009. doi: 10.2140/camcos.2009.4.27.
- [14] A. Christlieb, M. Morton, B. Ong, and J.-M. Qiu. Semi-implicit integral deferred correction constructed with additive Runge–Kutta methods. *Communications in Mathematical Sciences*, 9(3):879–902, 2011. doi: $10.4310/\mathrm{cms}.2011.\mathrm{v9.n3.a10}$.
- [15] A. J. Christlieb, Y. Liu, and Z. Xu. High order operator splitting methods based on an integral deferred correction framework. *Journal of Computational Physics*, 294:224–242, 2015. doi: 10.1016/j.jcp.2015.03.032.
- [16] P. Deuflhard and F. Bornemann. *Scientific Computing with Ordinary Differential Equations*. Springer New York, 2002. ISBN 9780387215822. doi: 10.1007/978-0-387-21582-2.
- [17] J. Donea. A taylor–galerkin method for convective transport problems. *International Journal for Numerical Methods in Engineering*, 20(1):101–119, 1984. doi: $10.1002/\mathrm{nme}.1620200108$.
- [18] A. Dutt, L. Greengard, and V. Rokhlin. Spectral deferred correction methods for ordinary differential equations. *Bit Numerical Mathematics*, 40(2):241–266, 2000. doi: 10.1023/a: 1022338906936.
- [19] N. Fehn, W. A. Wall, and M. Kronbichler. On the stability of projection methods for the incompressible Navier-Stokes equations based on high-order discontinuous Galerkin discretizations. *Journal of Computational Physics*, 351:392–421, 2017. doi: 10.1016/j.jcp.2017.09.031.
- [20] J. Frank, W. Hundsdorfer, and J. Verwer. On the stability of implicit-explicit linear multistep methods. *Applied Numerical Mathematics*, 25(2-3):193–205, 1997. doi: 10.1016/s0168-9274(97)00059-7.
- [21] P. Frolkovič and M. Žeravý. High resolution compact implicit numerical scheme for conservation laws. *Applied Mathematics and Computation*, 442:127720, 2023. doi: $10.1016/\mathrm{j.amc.}2022.$ 127720.
- [22] J. Glaubitz, A. C. Nogueira, J. L. S. Almeida, R. F. Cantão, and C. A. C. Silva. Smooth and compactly supported viscous sub-cell shock capturing for discontinuous galerkin methods. *Journal of Scientific Computing*, 79(1):249–272, 2019. doi: 10.1007/s10915-018-0850-3.

- [23] G. H. Golub and Q. Ye. Inexact preconditioned conjugate gradient method with inner-outer iteration. *SIAM Journal on Scientific Computing*, 21(4):1305–1320, 1999.
- [24] S. Gottlieb. On high order strong stability preserving Runge-Kutta and multi step time discretizations. *Journal of Scientific Computing*, 25(1–2):105–128, 2005. doi: 10.1007/bf02728985.
- [25] S. Gottlieb and D. Ketcheson. *Time Discretization Techniques*, pages 549–583. Elsevier, 2016. doi: 10.1016/bs.hna.2016.08.001.
- [26] M. Guesmi, M. Grotteschi, and J. Stiller. Assessment of high-order imex methods for incompressible flow. *International Journal for Numerical Methods in Fluids*, 95(6):954–978, 2023. doi: $10.1002/\mathrm{fld}.5177$.
- [27] T. Hagstrom and R. Zhou. On the spectral deferred correction of splitting methods for initial value problems. *Communications in Applied Mathematics and Computational Science*, 1(1):169–205, 2006. doi: 10.2140/camcos.2006.1.169.
- [28] E. Hairer and G. Wanner. *Solving Ordinary Differential Equations II*. Springer Berlin Heidelberg, 1996. doi: 10.1007/978-3-642-05221-7.
- [29] E. Hairer, S. P. Nørsett, and G. Wanner. *Solving Ordinary Differential Equations I*. Springer Berlin Heidelberg, 1993. doi: 10.1007/978-3-540-78862-1.
- [30] A. C. Hansen and J. Strain. On the order of deferred correction. *Applied Numerical Mathematics*, 61(8):961-973, 2011. doi: 10.1016/j.apnum.2011.04.001.
- [31] A. Harten and J. M. Hyman. Self adjusting grid methods for one-dimensional hyperbolic conservation laws. *Journal of Computational Physics*, 50(2):235–269, 1983. doi: 10.1016/0021-9991(83)90066-9.
- [32] M. R. Hestenes and E. Stiefel. Methods of conjugate gradients for solving linear systems. *Journal of research of the National Bureau of Standards*, 49(6):409–436, 1952.
- [33] J. S. Hesthaven and T. Warburton. *Nodal Discontinuous Galerkin Methods*. Springer, 2008.
- [34] T. J. R. Hughes and M. Mallet. A new finite element formulation for computational fluid dynamics: III. The generalized streamline operator for multidimensional advective-diffusive systems. *Computer Methods in Applied Mechanics and Engineering*, 58:305–328, 1986.
- [35] W. Hundsdorfer and J. Verwer. *Numerical Solution of Time-Dependent Advection-Diffusion-Reaction Equations*. Springer Berlin Heidelberg, 2003. doi: 10.1007/978-3-662-09017-6.
- [36] H. T. Huynh. Discontinuous Galerkin and related methods for ODE. *Journal of Scientific Computing*, 96(2), 2023. doi: 10.1007/s10915-023-02233-2.
- [37] G. Izzo and Z. Jackiewicz. Highly stable implicit–explicit runge–kutta methods. *Applied Numerical Mathematics*, 113:71–92, 2017. doi: 10.1016/j.apnum.2016.10.018.
- [38] B. Janssen and G. Kanschat. Adaptive multilevel methods with local smoothing for h^1 and $h^{\rm curl}$ -conforming high order finite element methods. *SIAM Journal on Scientific Computing*, 33 (4):2095–2114, 2011. doi: 10.1137/090778523.
- [39] A. Jaust, J. Schütz, and D. C. Seal. Implicit multistage two-derivative Discontinuous Galerkin schemes for viscous conservation laws. *Journal of Scientific Computing*, 69(2):866–891, 2016. doi: 10.1007/s10915-016-0221-x.
- [40] G. E. Karniadakis, M. Israeli, and S. A. Orszag. High-order splitting methods for the incompressible Navier-Stokes equations. *Journal of Computational Physics*, 97(2):414–443, 1991. doi: 10.1016/0021-9991(91)90007-8.
- [41] C. A. Kennedy and M. H. Carpenter. Additive Runge-Kutta schemes for convection-diffusion-reaction equations. *Applied Numerical Mathematics*, 44(1-2):139–181, 2003. doi: 10.1016/s0168-9274(02)00138-1.
- [42] C. A. Kennedy and M. H. Carpenter. Diagonally implicit runge–kutta methods for ordinary differential equations: A review. Technical Report NASA/TM 2016-219173, NASA, 2016.

- [43] D. I. Ketcheson. Highly efficient strong stability-preserving Runge–Kutta methods with low-storage implementations. *SIAM Journal on Scientific Computing*, 30(4):2113–2136, 2008. doi: 10.1137/07070485x.
- [44] B. Klein, F. Kummer, M. Keil, and M. Oberlack. An extension of the SIMPLE based discontinuous Galerkin solver to unsteady incompressible flows. *International Journal for Numerical Methods in Fluids*, 77(10):571–589, 2015. doi: 10.1002/fld.3994.
- [45] A. Klöckner, T. Warburton, and J. S. Hesthaven. Viscous shock capturing in a time-explicit Discontinuous Galerkin method. *Mathematical Modelling of Natural Phenomena*, 6(3):57–83, 2011. doi: 10.1051/mmnp/20116303.
- [46] P. Lax and B. Wendroff. Systems of conservation laws. *Communications on Pure and Applied Mathematics*, 13(2):217–237, 1960. doi: 10.1002/cpa.3160130205.
- [47] A. Layton and M. Minion. Implications of the choice of predictors for semi-implicit Picard integral deferred correction methods. *Communications in Applied Mathematics and Computational Science*, 2(1):1–34, 2007. doi: $10.2140/\mathrm{camcos.}2007.2.1$.
- [48] A. T. Layton and M. L. Minion. Implications of the choice of quadrature nodes for Picard integral deferred corrections methods for ordinary differential equations. *BIT Numerical Mathematics*, 45(2):341–373, 2005. doi: 10.1007/s10543-005-0016-1.
- [49] J. W. Lottes and P. F. Fischer. Hybrid multigrid/Schwarz algorithms for the spectral element method. *Journal of Scientific Computing*, 24(1):45–78, 2005. doi: 10.1007/s10915-004-4787-3.
- [50] E. Macca and S. Boscarino. Semi-implicit-type order-adaptive cat2 schemes for systems of balance laws with relaxed source term. *Communications on Applied Mathematics and Computation*, 2024. doi: 10.1007/s42967-024-00414-w.
- [51] M. Minion and R. Saye. Higher-order temporal integration for the incompressible Navier-Stokes equations in bounded domains. *Journal of Computational Physics*, 375:797–822, 2018. doi: 10.1016/j.jcp.2018.08.054.
- [52] M. L. Minion. Semi-implicit spectral deferred correction methods for ordinary differential equations. *Communications in Mathematical Sciences*, 1(3):471–500, 2003. doi: $10.4310/\mathrm{cms}$. 2003.v1.n3.a6.
- [53] B. W. Ong and R. J. Spiteri. Deferred correction methods for ordinary differential equations. *Journal of Scientific Computing*, 83(3), 2020. doi: 10.1007/s10915-020-01235-8.
- [54] Y. Pan, Z.-G. Yan, J. Peiró, and S. J. Sherwin. Development of a balanced adaptive time-stepping strategy based on an implicit JFNK-DG compressible flow solver. *Communications on Applied Mathematics and Computation*, 2021. doi: 10.1007/s42967-021-00138-1.
- [55] W. Pazner and P.-O. Persson. Stage-parallel fully implicit runge–kutta solvers for discontinuous galerkin fluid simulations. *Journal of Computational Physics*, 335:700–717, 2017. doi: 10.1016/j.jcp.2017.01.050.
- [56] P.-O. Persson and J. Peraire. Sub-cell shock capturing for Discontinuous Galerkin methods. In *44th AlAA Aerospace Sciences Meeting and Exhibit*. American Institute of Aeronautics and Astronautics, 2006. doi: 10.2514/6.2006-112.
- [57] A. Safjan and J. Oden. High-order Taylor-Galerkin methods for linear hyperbolic systems. *Journal of Computational Physics*, 120(2):206–230, 1995. doi: 10.1006/jcph.1995.1159.
- [58] J. Schütz and D. C. Seal. An asymptotic preserving semi-implicit multiderivative solver. *Applied Numerical Mathematics*, 160:84–101, 2021. doi: 10.1016/j.apnum.2020.09.004.
- [59] J. R. Shewchuk. An introduction to the conjugate gradient method without the agonizing pain. Technical report, Pittsburgh, PA, USA, 1994.
- [60] C.-W. Shu and S. Osher. Efficient implementation of essentially non-oscillatory shock-capturing schemes. *Journal of Computational Physics*, 77(2):439–471, 1988. doi: 10.1016/

- 0021-9991(88)90177-5.
- [61] C.-W. Shu and S. Osher. Efficient implementation of essentially non-oscillatory shock-capturing schemes, ii. *Journal of Computational Physics*, 83(1):32–78, 1989. doi: 10.1016/0021-9991(89)90222-2.
- [62] G. A. Sod. A survey of several finite difference methods for systems of nonlinear hyperbolic conservation laws. *Journal of Computational Physics*, 27(1):1–31, 1978. doi: 10.1016/0021-9991(78)90023-2.
- [63] R. Speck, D. Ruprecht, M. Emmett, M. Minion, M. Bolten, and R. Krause. A multi-level spectral deferred correction method. *BIT Numerical Mathematics*, 55(3):843–867, 2015. doi: 10.1007/s10543-014-0517-x.
- [64] J. Stiller. Nonuniformly weighted Schwarz smoothers for spectral element multigrid. *Journal of Scientific Computing*, 72(1):81–96, 2016. doi: 10.1007/s10915-016-0345-z.
- [65] J. Stiller. Robust multigrid for high-order discontinuous Galerkin methods: A fast Poisson solver suitable for high-aspect ratio Cartesian grids. *Journal of Computational Physics*, 327: 317–336, 2016. doi: 10.1016/j.jcp.2016.09.041.
- [66] J. Stiller. A spectral deferred correction method for incompressible flow with variable viscosity. *Journal of Computational Physics*, 423:109840, 2020. doi: $10.1016/\mathrm{j.jcp.}2020.109840$.
- [67] M. Tavelli and M. Dumbser. Arbitrary high order accurate space–time discontinuous Galerkin finite element schemes on staggered unstructured meshes for linear elasticity. *Journal of Computational Physics*, 366:386–414, 2018. doi: 10.1016/j.jcp.2018.03.038.